

Review Article

Open Access



# Advances in second-generation high-temperature superconducting tapes and their applications in high-field magnets

Kai Wang<sup>1,2,#</sup>, Hao Dong<sup>1,2,#</sup>, Daxing Huang<sup>1,2</sup>, Hongjing Shang<sup>1,2</sup>, Bowei Xie<sup>1,2</sup>, Qi Zou<sup>1,2</sup>, Lin Zhang<sup>1,2</sup>, Changping Feng<sup>1,2</sup>, Hongwei Gu<sup>1,2,\*</sup>, Fazhu Ding<sup>1,2,\*</sup>

<sup>1</sup>Key Laboratory of Applied Superconductivity and Institute of Electrical Engineering, Chinese Academy of Sciences, Beijing 100190, China.

<sup>2</sup>University of Chinese Academy of Sciences, Beijing 100049, China.

#Contributed equally.

\***Correspondence to:** Prof. Hongwei Gu, Key Laboratory of Applied Superconductivity and Institute of Electrical Engineering, Chinese Academy of Sciences, 6 Beiertiao Road, Haidian District, Beijing 100190, China. E-mail: guhw@mail.iee.ac.cn; Prof. Fazhu Ding, Key Laboratory of Applied Superconductivity and Institute of Electrical Engineering, Chinese Academy of Sciences, 6 Beiertiao Road, Haidian District, Beijing 100190, China. E-mail: dingfazhu@mail.iee.ac.cn

**How to cite this article:** Wang K, Dong H, Huang D, Shang H, Xie B, Zou Q, Zhang L, Feng C, Gu H, Ding F. Advances in second-generation high-temperature superconducting tapes and their applications in high-field magnets. *Soft Sci* 2022;2:12. <https://dx.doi.org/10.20517/ss.2022.10>

**Received:** 18 May 2022 **First Decision:** 26 May 2022 **Revised:** 15 Jun 2022 **Accepted:** 13 Jul 2022 **Published:** 1 Aug 2022

**Academic Editor:** Zhifeng Ren **Copy Editor:** Fangling Lan **Production Editor:** Fangling Lan

## Abstract

Second-generation high-temperature superconducting (2G-HTS) tapes based on REBa<sub>2</sub>Cu<sub>3</sub>O<sub>7-x</sub> (REBCO, RE: rare earth) materials enable the energy-efficient and high-power-density delivery of electricity, thereby promoting the development of clean energy generation, conversion, transmission, and storage. To overcome the weak grain-boundary connection and poor mechanical properties of these superconductors, a thin-film technology for epitaxy and biaxial textures based on flexible substrates has been developed. In recent years, high-quality 2G-HTS tapes have been produced at the kilometer scale and used in superconducting demonstration projects. This review first summarizes the development of HTS materials and briefly expounds the properties of REBCO superconducting materials. Subsequently, the structural characteristics, preparation methods, and current research progress of 2G-HTS tapes are given. In addition, the applications of REBCO tapes in constructing high-field magnets are also briefly reviewed.



© The Author(s) 2022. **Open Access** This article is licensed under a Creative Commons Attribution 4.0 International License (<https://creativecommons.org/licenses/by/4.0/>), which permits unrestricted use, sharing, adaptation, distribution and reproduction in any medium or format, for any purpose, even commercially, as long as you give appropriate credit to the original author(s) and the source, provide a link to the Creative Commons license, and indicate if changes were made.



**Keywords:** 2G-HTS tapes, REBCO, flux pinning, high-field magnets

## INTRODUCTION

The Dutch cryogenic physicist Onnes H. K. succeeded in liquefying helium and obtained a low temperature of 4.2 K in 1908, thereby enabling the later successful observation of superconductivity in Hg<sup>[1,2]</sup>. In subsequent decades, superconductivity has also been observed in many metallic elements and alloys. More importantly, new physical properties related to superconductivity, e.g., complete diamagnetism, the Josephson effect, and so on, have been realized<sup>[3-6]</sup>. This has helped to embed the application of superconducting techniques in many key areas. The phenomenological theory of superconductors and the microscopic theory of low-temperature superconductivity were proposed successively to predict the upper limit of the critical temperature ( $T_c$ ) of traditional superconductors<sup>[7,8]</sup>. In 1986, Bednorz and Muller of IBM in Switzerland discovered the existence of superconductivity in the La-Ba-Cu-O system, which opened a new chapter in the exploration of superconductivity in layered copper oxides<sup>[9]</sup>. In 1987, the discovery of the yttrium barium copper oxide (YBa<sub>2</sub>Cu<sub>3</sub>O<sub>7-δ</sub>, YBCO) high-temperature superconducting (HTS) material raised the  $T_c$  above the temperature of liquid N<sub>2</sub> and created a new era for research into HTS materials<sup>[10,11]</sup>. HTS materials with practical value mainly include BSCCO [ $T_c = \sim 90-110$  K, known as the first generation of HTS materials, e.g., Bi<sub>2</sub>Sr<sub>2</sub>CaCu<sub>2</sub>O<sub>8</sub> (BSCCO-2212) and Bi<sub>2</sub>Sr<sub>2</sub>Ca<sub>2</sub>Cu<sub>3</sub>O<sub>10</sub> (BSCCO-2223)<sup>[12,13]</sup>] and REBCO<sup>[14-16]</sup> ( $T_c = \sim 93$  K, also known as HTS-coated conductors, with YBCO as the representative example). Since the beginning of the 21<sup>st</sup> century, MgB<sub>2</sub> ( $T_c = 39$  K)<sup>[17-19]</sup> and Fe-based superconductors ( $T_c$  of up to 55 K)<sup>[20-22]</sup> have become two new kinds of low-cost superconductors.

Compared with BSCCO, REBCO has a higher critical current density ( $J_c$ ) and irreversible field. REBCO also has a higher  $T_c$  than MgB<sub>2</sub>- and Fe-based superconductors and does not contain toxic elements compared with other types of copper oxide- (e.g., Hg and Tl series<sup>[23-25]</sup>) and Fe-based superconductors. A three-dimensional diagram of the  $T_c$ , upper critical field ( $B_{c2}$ ) and  $J_c$  of various practical superconducting materials (including NbTi, MgB<sub>2</sub>, Bi2223 and YBCO) is shown in Figure 1<sup>[26]</sup>. It can be seen that YBCO tapes have higher  $J_c$  in a larger range of temperatures and magnetic fields. Therefore, second-generation (2G)-HTS tapes are more promising for commercial applications and have become one of the most widely and deeply researched types of superconducting materials<sup>[27-33]</sup>.

In this review, the structures and characteristics of REBCO and 2G-HTS tapes are first introduced. The challenges facing 2G-HTS tapes in recent years (especially in flux pinning) are then described and the research progress in addressing them is also summarized. We then present the high-magnetic field application of 2G-HTS tapes, which are usually used as insert magnets due to their higher critical transition field. In addition, the closed-loop operation of 2G-HTS tapes has excellent characteristics of stability and almost no current attenuation. It generates a magnetic field of high homogeneity and stability necessary for Nuclear Magnetic Resonance (NMR) and Magnetic Resonance Imaging (MRI)<sup>[34]</sup>. Finally, the research progress of 2G-HTS tapes in superconducting magnets in different research groups worldwide, including the National High Magnetic Field Laboratory (NHMFL), SuNAM Co Ltd (SuNAM), the RIKAGAKU KENKYUSHO/Institute of Physical and Chemical Research (REKIN), and the Institute of Electrical Engineering of the Chinese Academy of Sciences (IEECAS), is reviewed.

## CHARACTERISTICS OF REBCO

The performance of 2G-HTS tapes is mainly determined by the quality of the REBCO layer. REBa<sub>2</sub>Cu<sub>3</sub>O<sub>7-x</sub> has a layered two-dimensional (2D) structure that is derived from the perovskite structure [Figure 2]<sup>[35]</sup>. The lattice constants of YBCO-type HTS materials are  $a = 0.3821$  nm,  $b = 0.3885$  nm and  $c = 1.1680$  nm. The

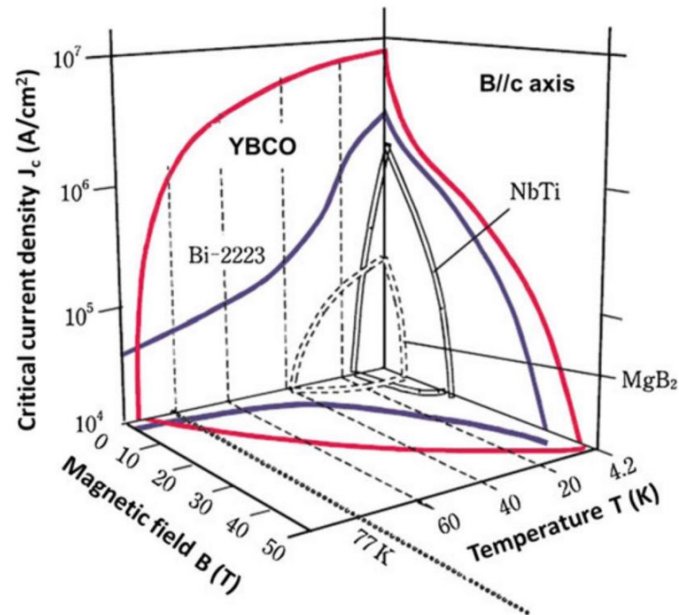


**Figure 1.** 3D diagrams of  $T_c$ ,  $B_{c2}$  and  $J_c$  of various superconductors (including NbTi,  $MgB_2$ , YBCO and Bi-2223)<sup>[26]</sup> © 2017 Springer International Publishing AG.

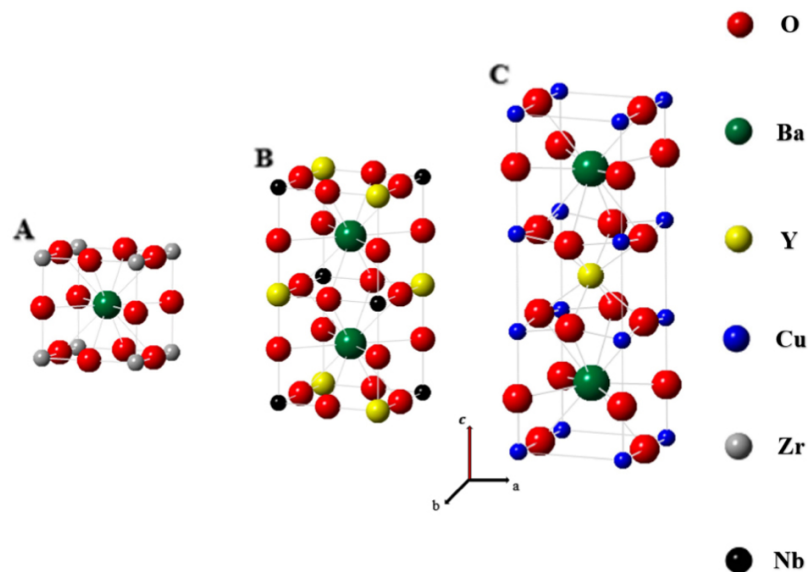


**Figure 2.** (A) Crystal structures of single-perovskite  $ABO_3$ , e.g.,  $BaZrO_3$  (BZO). (B) Crystal structures of double-perovskite  $A_2BB'O_6$ , e.g.,  $Ba_2YNbO_6$  (BYNO) and  $Ba_2YTaO_6$  (BYTO). (C) Crystal structures of REBCO, e.g., YBCO and GDBCO<sup>[35]</sup> © 2017 IOP Publishing Ltd. Printed in the UK.

lattice constants of gadolinium barium copper oxide-type (GdBCO) HTS materials are  $a = 0.3849$  nm,  $b = 0.3909$  nm and  $c = 1.1682$  nm<sup>[36-40]</sup>. The above data show that the  $c$  lattice constant of REBCO is three to four times the  $a$  or  $b$  lattice constant. Furthermore, the superconducting energy gap of copper oxide-based HTS materials has  $d$ -wave symmetry with strong anisotropy. Therefore, 2G-HTS tapes have obvious anisotropy, which causes difficulties for their applications. The penetration depth ( $\lambda$ ) of REBCO is much longer than the coherence length ( $\xi$ ), and its Meissner effect is incomplete. In the mixed state, the flux lines

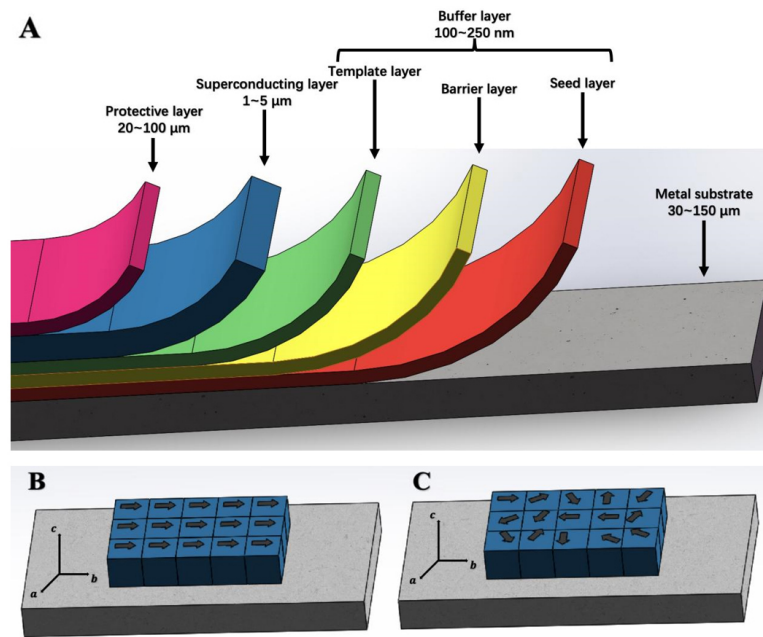


**Figure 3.** (A) Schematic diagram of the typical structure of 2G-HTS tape. (B) Schematic diagram of the uniaxial texture of grains in a polycrystalline system. (C) Schematic diagram of the biaxial texture of grains in a polycrystalline system.

pass through REBCO in the form of a flux quantum beam. Moreover, the flux lines flow and anisotropy become more obvious due to the high working temperature and large thermal disturbance of 2G-HTS tapes. An effective method to solve this problem is to introduce various pinning centers to bind the flux lines. REBCO superconductors have a small  $\xi$ , so a large angle grain boundary could cause a weak connection that blocks the superconducting current. To avoid this problem, various methods have been proposed to solve the biaxial texture problem, including a variety of film preparation methods. These methods are used to prepare excellent REBCO layers with biaxial texture and c-axis orientation.

As ceramic materials, it is difficult to prepare high-performance 2G-HTS tapes that have excellent mechanical properties and meet the numerous required engineering applications using REBCO. In addition, the internal stress generated during the growth process of REBCO also significantly impacts the performance of 2G-HTS tapes. The service condition of REBCO tapes usually involves an alternating-current field and a magnetic field, which cause energy loss to the superconductor. The tape width, pinning center, and protective layer can be tuned to address the above problems effectively. Increasing the thickness of the REBCO layer is the primary consideration for improving the engineering current density ( $J_e$ ) and reducing the cost of 2G-HTS tapes. These efforts are detailed in the next section.

## RESEARCH STATUS OF 2G-HTS TAPES

### Structure and preparation methods of 2G-HTS tapes

Figure 3A shows a typical 2G-HTS tape structure, which is generally composed of a metallic substrate, a buffer layer, a superconducting layer, and a protective layer (the buffer layer is usually composed of a seed layer, a barrier layer and a template layer). As mentioned above, in the preparation process of 2G-HTS tapes, high-angle grain boundaries in the REBCO layer have to be avoided by biaxial texture, i.e., the grains of REBCO should be orderly arranged in the a-b plane and c-axis direction (uniaxial and biaxial textures, as shown in Figure 3B and C, respectively). Unlike metallic superconducting materials, 2G-HTS tapes are poor in ductility and machinability, because of the ceramic REBCO layer. Therefore, these tapes are usually

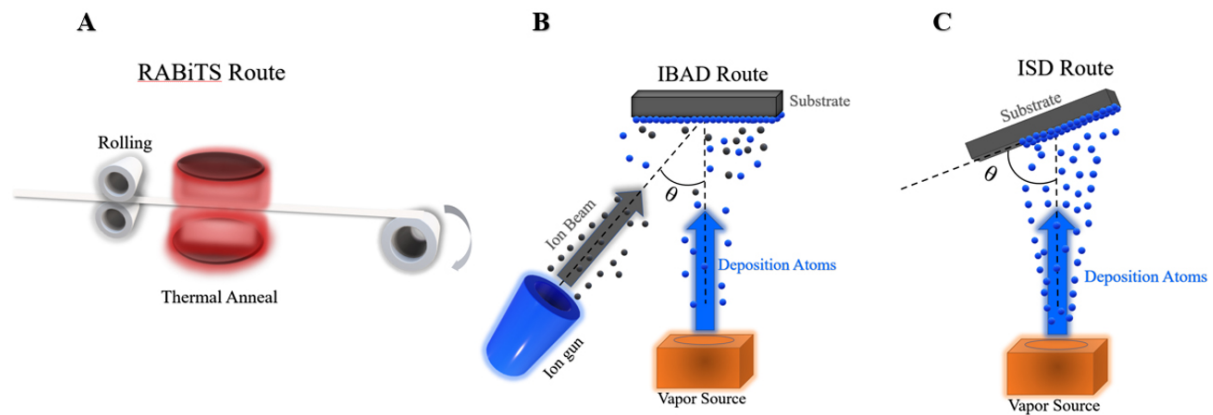


**Figure 4.** Schematic diagram of three methods to obtain substrates with biaxial texture. (A) RABiTS route is to roll flexible Ni or Ni-based alloys to obtain ribbon-like materials and then obtain biaxially textured grains by secondary crystallization through annealing. Ni or Ni-based alloy substrates with biaxial texture become templates for epitaxial growth of buffer layers (e.g.,  $\text{RE}_2\text{O}_3$ ,  $\text{CeO}_2$  and YSZ). (B) IBAD route uses ion beam-assisted techniques to obtain preferred orientation deposited films. Furthermore, biaxially textured oxide buffer layers, such as MgO, are grown on polycrystalline metal substrates, such as stainless steel. (C) ISD route is quite similar to IBAD route. The method of tilting the substrate is used to obtain preferentially oriented deposited films<sup>[41,42,55]</sup> © 2009 Elsevier B.V. All rights reserved; © 1993 American Institute of Physics; © 2005 Elsevier B.V. All rights reserved.

prepared on flexible metallic substrates with biaxial texture by epitaxial growth so that the excellent textural characteristics of the substrates are transmitted to the superconducting layer. There are three main methods to obtain substrates with biaxial texture (as shown in Figure 4<sup>[41,42]</sup>), namely, rolling-assisted biaxial texture substrate (RABiTS), ion beam-assisted deposition (IBAD), and inclined substrate deposition (ISD)<sup>[43-52]</sup>.

IBAD was proposed by Iijima *et al.* from the Fujikura Company in Japan in 1992 and formed after further development in Los Alamos National Laboratory in the United States<sup>[53]</sup>. In 1997, Wang *et al.* (Gintzon Laboratory, Stanford University) successfully made high-quality in-plane textured MgO films on amorphous  $\text{Si}_3\text{N}_4$  substrates using IBAD, which are promising structural templates for the fabrication of REBCO materials<sup>[48]</sup>. In short, IBAD is used to obtain biaxial texture using an ion beam to attack the non-textured substrate and make the deposited oxide film grow in orientation. RABiTS was developed by Oak Ridge National Laboratory in the United States in 1996, with a Ni alloy substrate with biaxial texture obtained by rolling with large deformation and annealing at high temperature<sup>[54]</sup>. ISD was proposed by Bauer *et al.* in 1999 and further developed by the Theva Company in Germany<sup>[52,55,56]</sup>. In this method, the deposition source and non-textured substrate are placed at a certain angle to obtain the textural orientation of the deposited oxide film. The biaxial texture is first obtained in the substrate and will then be effectively transferred to the superconducting layer, so that the design of the buffer layer is prioritized.

It is well known that oxygen and metal atoms diffuse quickly at high temperatures. Since the growth of REBCO thin films requires a high temperature and oxygen environment, oxidation of the metal substrate and damage to the superconducting layer can readily occur under these conditions. Therefore, the substrate requires a barrier layer to block atomic diffusion. The key to ensuring texture transfer is to provide a template layer with lattice matching for YBCO growth. The template and barrier layers are generally oxides, so a seed layer is needed to deposit on the surface of the metal substrate to help the crystallization and growth of oxides. In terms of the scheme selection of the buffer layer, the technical route of one, two, three, or even more layers is adopted<sup>[57-61]</sup>. The ultimate purpose is to play an influential role in preventing diffusion and providing a high-quality growth template. There are many kinds of preparation methods for the buffer layer, including physical and chemical deposition methods, such as magnetic control sputtering deposition (MCSD), IBAD, pulsed laser deposition (PLD), chemical solution deposition, metal-organic

**Table 1. Comparison of characteristics of four main thin-film preparation methods for epitaxial growth of superconducting layer**

	Chemical methods		Physical methods	
	MOD	MOCVD	RCE	PLD
Characteristic	Ectopic growth	In-situ growth	Ectopic growth	In-situ growth
Advantages	Low cost of equipment; Easily controlled stoichiometry; 100% utilization of raw materials	Large sedimentation area; High film density; Fast production rate	High efficiency; Large sedimentation area; High material density	Simple target material; High film density; Simple process
Disadvantages	Technical difficulty; Relatively many defects	High phase forming temperature; Expensive raw materials	Difficult phase forming control; Weak flux pinning	High cost of equipment; Slow film growth

chemical vapor deposition (MOCVD), and metal-organic deposition (MOD). In addition, after the texture layer is grown by ISD and IBAD, it generally has an excellent blocking effect, so only the template layer for the growth of REBCO film needs to be deposited.

The superconducting layer is the key to determining the performance of 2G-HTS tapes. Currently, the main preparation methods for the REBCO superconducting layer are PLD, MOCVD, reactive electron beam co-evaporation (RCE), and MOD. These methods can be used to prepare 2G-HTS tapes with excellent properties, with each method having its own advantages and disadvantages. For example, the deposition rate of PLD and MOCVD is relatively fast, while PLD and MOD have the characteristics of a high utilization rate of raw materials. At present, these methods have been used in the preparation of commercial 2G-HTS tapes. MOCVD has certain advantages in preparation efficiency, while MOD has more market potential for cost reduction (a detailed comparison is shown in [Table 1](#)<sup>[62]</sup>).

The protective layer generally refers to the superconducting layer coated with a layer of Ag, Cu, or a combination of the two. The role of the protective layer can be divided into the following three points: (1) protecting the REBCO superconducting layer from environmental pollution; (2) carrying current when the REBCO layer loses its superconducting state; (3) connecting lead in practical applications. The protective layer is usually deposited by MCSD and electroplating technology.

### Development process of 2G-HTS tapes

To meet practical requirements, the length of 2G-HTS tapes and their current-carrying capacity have to be increased, while the preparation cost must be reduced to compete with other types of superconductors (e.g., NbTi and Nb<sub>3</sub>Sn) to achieve large-scale commercialization applications. In 1999, 2G-HTS tapes of 100 m in length were produced for the first time. After tremendous efforts focused on production routes and equipment in the past twenty years, there is now the capability of producing high current-carrying capacity tapes on a kilometer scale. SuperPower in the United States made the first kilometer-scale REBCO tape through the IBAD+MOCVD route in 2007, with its critical current ( $I_c$ ) reaching 300 A/cm<sup>[63,64]</sup>. In recent years, the company has continuously worked on the thickness reduction of the substrate to obtain 2G-HTS tapes with higher current-carrying capacity. SuNAM in South Korea began to fabricate 2G-HTS tapes in 2004 and in 2014 produced 660 m tapes of GdBCO with an  $I_c$  exceeding 620 A/cm through a RCE-deposition and reaction process. The overall processing speed of the 2G-HTS tapes can reach 120 m/h, and through the self-designed RGB color analysis method, the average  $I_c$  is increased to 561 A/cm (the uniformity of  $I_c$  reaches 95%)<sup>[65,66]</sup>. In 2009, the American Superconducting Corporation (AMSC) produced 2G-HTS tapes with an  $I_c$  of 260 A/cm and a length of 500 m using a low-cost MOD method<sup>[67]</sup>. In 2011, Fujikura in Japan used the IBAD+PLD route to prepare 2G-HTS tapes with a length of 816 m, with an average  $I_c$  of 572 A/cm.

**Table 2. Research progress of commercial 2G-HTS tapes<sup>[68-72]</sup>**

Continent	R&D and production institution (country)	Buffer layer and rebuffer layer epitaxial route	Single tape current-carrying Record (Year)	Current-carrying capacity of tapes under magnetic field (B//c)
Asia	SuNAM (South Korea)	IBAD + RCE	275 A / 470 m (2010) 355 A / 920 m (2011) 422 A / 1000 m (2012) 579 A / 978 m (2014) 625 A / 1000 m (2015)	$I_c(4.2\text{ K}, 18\text{ T}) > 115\text{ A}$ (2017)
	Fujikura (Japan)	IBAD + PLD	306 A / 368 m (2007) 350 A / 504 m (2008) 572 A / 816 m (2011) 580 A / 1040 m (2012)	$I_c(4.2\text{ K}, 18\text{ T}) \approx 750\text{ A}$ (2020)
	SWCC (Japan)	IBAD + MOD	310 A / 500 m (2008)	$I_c(4.2\text{ K}, 18\text{ T}) > 125\text{ A}$ (2018)
	Samri (China)	IBAD + MOCVD	150 A / 1000 m (2014) 570 A / 1130 m (2016)	$I_c(4.2\text{ K}, 10\text{ T}) = 710\text{ A}$ (2022)
	SCSC (China)	IBAD + MOD	350 A / 500 m (2018)	$I_c(4.2\text{ K}, 12\text{ T}) = 300\text{ A}$ (2022)
	SST (China)	IBAD + PLD	550 A / 1000 m (2018)	$I_c(4.2\text{ K}, 18\text{ T}) = 450\text{ A}$ (2019)
	North America	SuperPower (America)	IBAD + MOCVD	173 A / 595 m (2007) 153 A / 1311 m (2008) 282 A / 1065 m (2009)
AMSC (America)		RABiTS + MOD	466 A / 540 m (2010)	$I_c(4.2\text{ K}, 18\text{ T}) > 110\text{ A}$ (2018)
Europe	Bruker (Germany)	ABAD + PLD	260 A / 100 m (2009) 350 A / 270 m (2014) 330 A / 600 m (2016)	$I_c(4.2\text{ K}, 18\text{ T}) = 454\text{ A}$ (2019)

Although Chinese competitors entered the area of 2G-HTS tapes later, their products could match those of pioneering companies. For example, in 2017, the Institute of Suzhou Advanced Materials (Samri) and IEECAS jointly prepared 2G-HTS tapes with a length of 1130 m, with the average  $I_c$  reaching 570 A/cm using the IBAD+MOCVD route. Table 2 presents a more comprehensive and detailed development process of 2G-HTS tapes<sup>[68-71]</sup>. Bruker in Germany uses the alternate beam-assisted deposition (ABAD)-PLD route to prepare 2G-HTS tapes. It is committed to improving the current-carrying capacity of tapes at low temperatures and high fields<sup>[72]</sup>. At present, the  $I_c$  per unit width of 2G-HTS tapes prepared by most companies exceeds 300 A/cm at 77 K and self-field (s.f.) conditions, with the  $I_c$  of 100-m-class 4 mm wide product 2G-HTS tapes having reached 100-200 A (77 K, s.f.). The MOD method requires low-cost acetate and low-temperature pyrolysis. The crystallization of the high-temperature REBCO superconducting layer and the oxygen absorption treatment of REBCO in the later stage do not require vacuum equipment. Therefore, the MOD method is the best comprehensive method in terms of cost for producing the superconducting layer at present. The transient liquid-phase-assisted growth mode<sup>[73]</sup> developed in recent years can realize the rapid growth of the superconducting layer (theoretical value of 100 nm/s)<sup>[74]</sup>. This greatly improves the production efficiency of the MOD route and can further effectively reduce the production cost of 2G-HTS tapes.

The thickness of the superconducting layer is only one percent of the thickness of the entire 2G-HTS tape. A simple concept is to increase the thickness of the superconducting layer to improve the superconducting properties of the 2G-HTS tape. Unfortunately, there is a “thickness effect” that is difficult to improve, where the  $J_c$  decreases exponentially with increasing superconducting layer thickness. It was found that the thickness effect may be caused by the non-uniform element diffusion at the interface, the deterioration of the microstructure, the crystallinity change and the surface roughness, and porous surface morphology, which lead to a decrease in superconducting performance<sup>[75-80]</sup>. However, Selvamanickam’s group at the University of Houston, USA, through high-density Zr doping, not only effectively improved the in-field performance, but also achieved a substantial increase in the  $F_p$  at 77 K, which also played a good role in overcoming the thickness effect. They prepared a superconducting layer with a thickness of 4.6  $\mu\text{m}$  (15% Zr

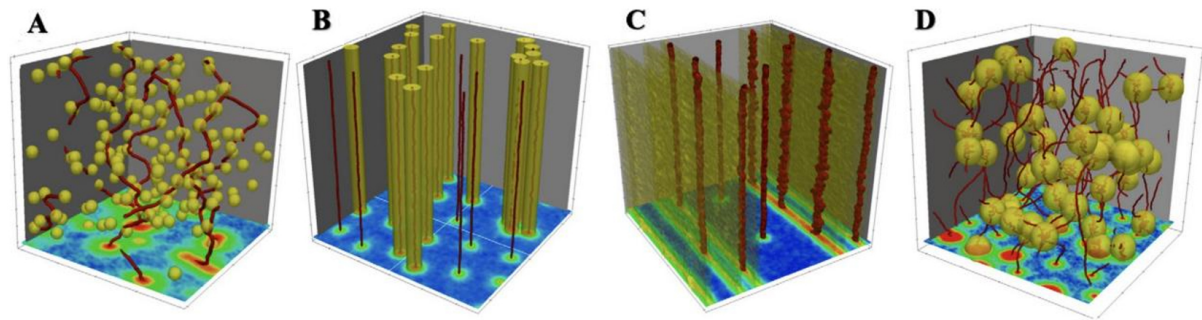


**Figure 5.** Schematic diagram of APCs with different dimensions in 2G-HTS tapes. (A) 0D atomic-level point defects, which mainly refer to defects smaller than  $\xi$ , usually with vacancies and element substitutions. (B) 1D defects (linear defects), including dislocations, self-assembled nanorods, and irradiated columnar defects. (C) 2D planar defects, including twin boundaries and stacking faults. (D) 3D large-size defects, including rare-earth oxide particles, secondary phase particles, defect clusters, and holes<sup>[89]</sup> © 2016 IOP Publishing Ltd. Printed in the UK.

doping) by the MOCVD route, maintaining a good orientation texture and  $J_c$ . Therefore, a 12 mm-wide tape was obtained with a  $J_c$  exceeding 1611 A (77 K, s.f.), achieving the effect that the critical current of the tape increases linearly with the thickness<sup>[81-83]</sup>. In 2020, they successfully prepared an optimized REBCO sample with 15% mol. Hf addition and 4.0  $\mu\text{m}$  thickness by using advanced MOCVD. The  $J_c$  performance at B//ab at 15 T is over 16 times higher than that of  $\text{Nb}_3\text{Sn}$ . The  $F_p$  at the B//ab orientation exceeds 10  $\text{TN m}^{-3}$  above 30 T, reaching 11.5  $\text{TN m}^{-3}$  at 31.2 T<sup>[84]</sup>. The modified RCE route adopted by the SuNAM can also greatly weaken the thickness effect, with their short 5  $\mu\text{m}$ -thick Sm123 thin films reaching a  $J_c$  of 1540 A/cm (77 K, s.f.)<sup>[85]</sup>.

### Research progress of flux pinning of 2G-HTS tapes

As a second-type (type-II) superconductor, the application circumstance of REBCO is usually between the lower critical field ( $H_{c1}$ ) and the upper critical field ( $H_{c2}$ ), i.e., the superconductor is in a mixed state. Since the interface energy between the normal state and the superconducting state of type-II superconductors is negative, flux lines in the mixed state of 2G-HTS tapes will pass through in the form of flux sub-beams. When the current flows through 2G-HTS tapes, the movement of the flux lines will generate a built-in electric field to cause loss and the disappearance of superconductivity. Therefore, type-II superconductors in a fully ideal state (i.e., without defects in the superconducting phase) can carry very few currents<sup>[86]</sup>. To improve the current-carrying capacity of 2G-HTS tapes, an effective pinning landscape must be introduced to form defects or energy potential wells to bind the flux lines. This has been the focus and difficulty in this field in recent years. The flux lines are simultaneously affected by the Lorentz and pinning forces, so a superconductor with a large pinning force has a relatively strong ability to transmit current. The pinning forces in the REBCO layer are mainly derived from the pinning effect of the layer structure (CuO plane) on flux lines (also known as the intrinsic pinning of the crystal structure) and the contribution of other in-plane defects, known as intrinsic pinning centers<sup>[75,87,88]</sup>. The artificial pinning centers (APCs) introduced into the REBCO layer from outside provide more pinning forces.

The introduction of APCs plays an irreplaceable role in improving the current-carrying capacity and adjusting the anisotropy of 2G-HTS tapes. As mentioned previously, the  $\xi$  is relatively short, so the size of the APCs must be controlled on the nanoscale in order to obtain an effective flux pinning effect. APCs can be divided into four categories in terms of morphology, namely, zero-dimensional (0D), one-dimensional (1D), 2D, and three-dimensional (3D) APCs (as shown in Figure 5<sup>[89]</sup>). The introduced APCs can be divided into magnetic and non-magnetic materials according to their functionality. The magnetic pinning forces generated by magnetic materials have a better pinning effect due to their special magnetic properties<sup>[90]</sup>.

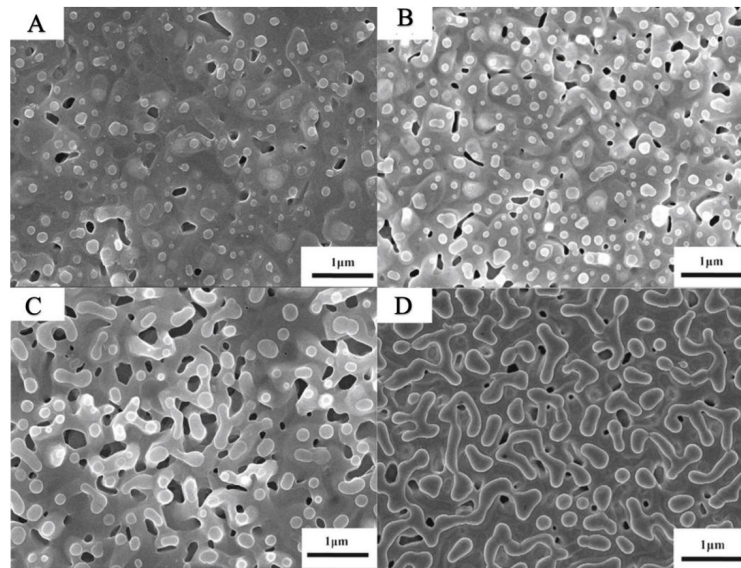


**Figure 6.** SEM images of superconducting layers with different Eu doping levels. (A) SEM image when Eu doping amount is 0. (B) SEM image when Eu doping amount is 0.1. (C) SEM image when Eu doping amount is 0.3. (D) SEM image when Eu doping amount is 0.5<sup>[98]</sup> © Springer Science+Business Media New York 2016.

Currently, there are four kinds of methods to introduce APCs into 2G-HTS tapes, namely, substrate surface modification, rare-earth element substitution, nano second-phase doping, and particle irradiation. In addition to single types of defects, a combination of two or three methods is also frequently adopted to introduce multiple defects, and there may be synergistic or competitive effects among defects<sup>[91-93]</sup>.

#### *Enhanced flux pinning by rare-earth element substitution*

This method relies on the lattice distortion energy caused by the difference in the atomic size of substitution to improve the flux pinning forces. In 1991, Jin *et al.* systematically studied the superconducting properties of the Y position of rare-earth elements in YBCO compounds after 20% atomic substitution and found that some rare-earth elements have an inhibitory effect on  $T_c$ <sup>[94]</sup>. Some rare-earth elements (e.g., Sm, Gd and Eu) can promote  $J_c$  after the substitution for Y. In the preparation of REBCO superconducting thin films, a large number of rare-earth elements (such as Dy and Gd) are employed for the substitution. Devi *et al.* successfully prepared  $Y_{1-x}Dy_xB_2Cu_3O_{7-\delta}$  thin films by using the PLD method to partially replace Y with Dy<sup>[95]</sup>. These films had the highest  $J_c$  at a 20% substitution of Dy for Y. The analysis of lattice defects induced by the stress field shows that this composition ( $Y_{0.8}Dy_{0.2}B_2Cu_3O_{7-\delta}$ ) is the optimum proportion to form effective flux pinning. Jin *et al.* also fabricated GdBCO films on  $LaAlO_3$  single crystal substrates with a  $T_c$  of 92.9 K (higher than pure YBCO films) and a  $J_c$  of 2.9 MA/cm<sup>2</sup><sup>[96]</sup>.

There are many studies on substituting Eu for other rare-earth elements. In 2007, Zhou *et al.* used PLD technology to prepare mixed REBCO superconducting films ( $Y_{0.67}Eu_{0.33}Ba_2Cu_3O_{7-\delta}$ ) with different thicknesses on single-crystal  $SrTiO_3$  (STO) substrates<sup>[97]</sup>. The microstructure of (Y, Eu)BCO films is improved by the introduction of Eu, and the films show better current-carrying performance than pure YBCO films over a wide range of orientations at low fields. One-third of the Y, substituted by Eu, may introduce sufficient strain for additional random pinning sites due to the ionic radius difference between Y and Eu. Li *et al.* used the MOCVD method to prepare Eu-doped YBCO films with a doping concentration of between 0 and 50%<sup>[98]</sup>. Scanning electron microscopy (SEM) images of the films with different doping levels are shown in Figure 6. The introduction of Eu results in superconducting films with many nanoparticles and pores with a

regular distribution on the surface. Moreover, the introduction of Eu also makes the surface of the YBCO film denser and smoother, with a larger  $J_c$  (especially when the Eu doping amount is greater than 0.1). Eu doping can not only form an effective pinning center, but also improves the connectivity between the grains of the superconducting layer. These results suggest that Eu doping is a promising approach to enhance  $J_c$  fundamentally. In practice, the flux pinning landscape produced by rare-earth element substitution is weaker than that of nano second-phase doping, but the  $J_c$  of REBCO superconducting thin films can be significantly improved through the synergistic effect of the two.

#### *Enhanced flux pinning through substrate surface modification*

Substrate surface modification refers to the depositing of metal or oxide nanoparticles on the substrate first before depositing the YBCO superconducting layer or depositing a nanoscale oxide film. It mainly produces linear (1D) defects to improve the performance of the tapes. In 2003, Nie *et al.* used the PLD method to grow YBCO thin films on CeO<sub>2</sub>-buffered (1 $\bar{1}$ 02) sapphire (Al<sub>2</sub>O<sub>3</sub>) substrates<sup>[99]</sup>. They induced the reconstruction of the surface structure of CeO<sub>2</sub> on Al<sub>2</sub>O<sub>3</sub> substrates by high-temperature (1025 °C) O<sub>2</sub> annealing treatment before depositing a superconducting film. A flat CeO<sub>2</sub> layer and self-assembled nanodots form on the surface of the buffer layer. The threading dislocations induced by CeO<sub>2</sub> nanodots and the high density of egg-shaped nanoscale precipitates extending along the c-axis of YBCO generate c-axis-related pinning sites, which enhance the flux pinning along the c-axis of the superconducting film. The properties of YBCO superconducting thin films prepared on the buffer layer were tested at different temperatures. When the magnetic field moves along the c-axis of YBCO, it exhibits a higher and broader  $J_c$  peak. Aytug *et al.* made a YBCO superconducting film with a  $J_c$  of  $6.6 \times 10^6$  A/cm<sup>2</sup> (77 K, s.f.) by depositing a layer of iridium nanodots with a thickness of 20 nm (150 nm in diameter) on the STO substrate in advance<sup>[100]</sup>. The  $J_c$  is at least 50% higher than that of the superconducting film deposited directly on the substrate. Baca *et al.* used Y<sub>2</sub>O<sub>3</sub> nanodot-modified substrates to fabricate YBCO films with superficially porous structures, which can play an effective role in flux pinning<sup>[101]</sup>. Mikheenko *et al.* deposited a large number of Ag nanoparticles on the surface of a STO substrate by the PLD method ( $10^{11}$ - $10^{12}$ /cm<sup>2</sup>), which can also generate defects along the c-axis in YBCO, thus significantly improving the  $J_c$ <sup>[102]</sup>.

Wang *et al.* used RF magnetron sputtering to make a surface modification on STO substrates to sputter randomly distributed La<sub>0.67</sub>Sr<sub>0.33</sub>MnO<sub>3</sub> (LSMO) particles with diameters of 10-20 nm and heights of 20-50 nm (an atomic force microscopy image of a LSMO nanoparticle is shown in [Figure 7A](#) and [B](#))<sup>[103]</sup>. The modification of the LSMO nanoparticles introduced c-axis-oriented linear dislocations throughout the superconducting layer to form 1D APCs in the film. [Figure 7C](#) clearly indicates that the GdBCO film fabricated on the LSMO-decorated substrate shows a larger  $J_c$  in the high region of the magnetic field ( $H \geq 1.3$  T) at 30 K. At 77 K, the GdBCO film fabricated on the LSMO-decorated substrate shows a larger  $J_c$  over the whole investigated region of the magnetic field, as shown in [Figure 7D](#). The main reason for this is the flux pinning forces in the superconducting layer due to the magnetic characteristics of the LSMO material and the pinning forces provided by the columnar 1D defects. Jha *et al.* used the PLD method to prepare YBCO superconducting films on a LSMO particle-modified STO substrate<sup>[104]</sup>. The  $J_c$  value of the YBCO films without the substrate surface modification was  $3.64 \times 10^4$  A/cm<sup>2</sup> (77 K, 4 T), while the  $J_c$  value of the YBCO films modified with LSMO nanoparticles was increased by one order of magnitude to  $1.44 \times 10^5$  A/cm<sup>2</sup> (77 K, 4 T). The defects introduced by the surface modification of the substrate are generally nanodefects along the c-axis, resulting in a good pinning effect in the c-axis direction and thus effectively reducing the anisotropy of the REBCO superconducting films.

#### *Enhanced flux pinning by particle irradiation*

Particle irradiation involves bombarding REBCO films or tapes with particles so that the atoms are

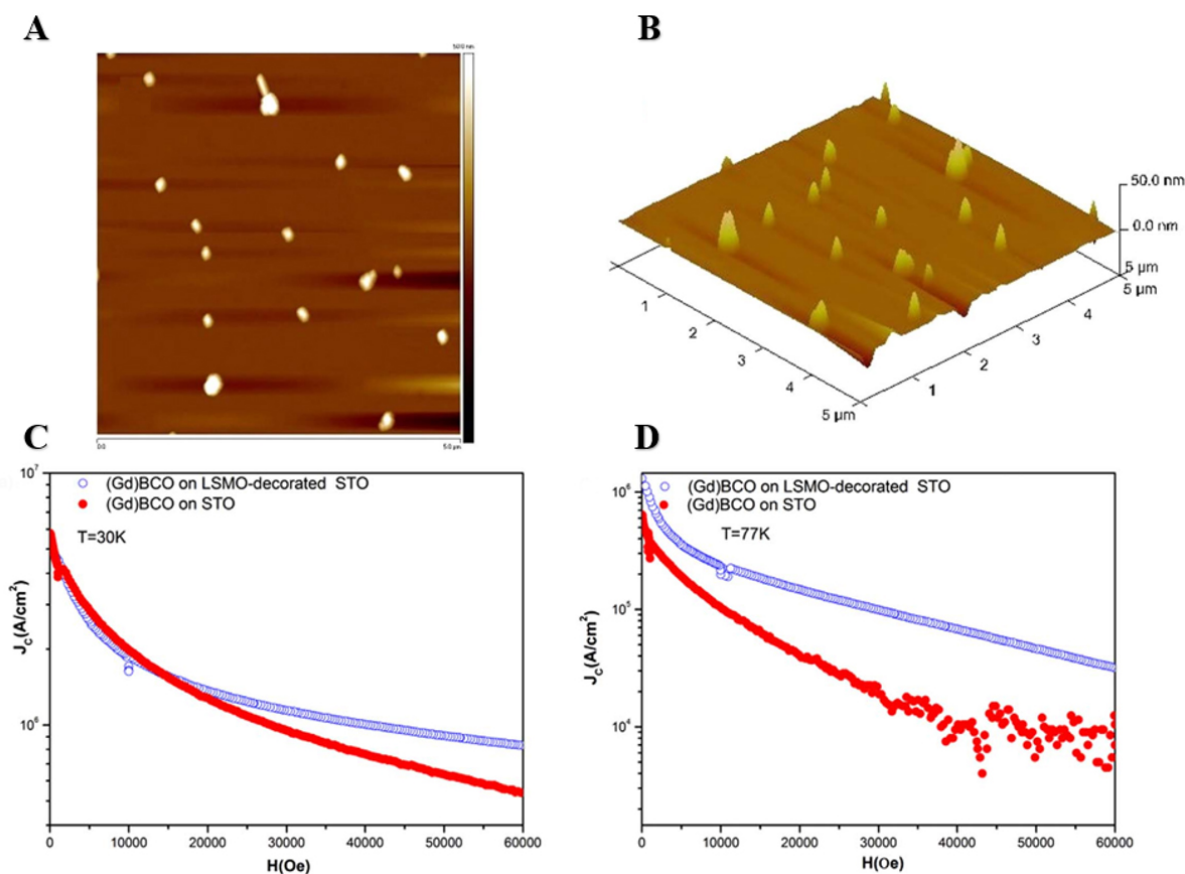


**Figure 7.** Atomic force microscopy image of LSMO nanoparticle-decorated STO substrates: (A) 2D and (B) 3D image. Field dependence of  $J_c$  for GdBCO thin films on undecorated and LSMO-decorated STO substrates at (C) 30 K and (D) 77 K<sup>[103]</sup> © 2017 Elsevier Ltd. and Techna Group S.r.l. All rights reserved.

dislocated to form defects. It mainly pins the flux by generating 1D pinning centers, thereby increasing the  $J_c$  in a wide range of magnetic field strengths and directions. In terms of irradiation, it belongs to the introduction of APCs by physical means. Compared with the traditional chemical doping method, particle irradiation can form various types and sizes of defects in the superconducting layer by controlling the types, energies, and radiation doses of irradiated particles without changing the stoichiometric ratio of the superconducting material. In general, particles, such as electrons, protons, neutrons, and heavy ions, can be used for irradiation. Matsui *et al.* irradiated a YBCO film with 3 MeV Fe ions and studied its superconductivity<sup>[105]</sup>. They found that the  $J_c$  of the YBCO film irradiated by Fe ions was increased by 70% in the presence of an external magnetic field. The authors irradiated YBCO tapes in the second year with 3 MeV Au ions. When the irradiation dose was  $1 \times 10^{11}/\text{cm}^2$ , the  $J_c$  (77 K, 6 T//c) increased nearly fourfold. They then irradiated 2G-HTS tapes with Si and B ions and the  $J_c$  of the tape increased 11-fold when a mixture of 70% 750 keV Si ions and 30% 200 keV B ions was used<sup>[106,107]</sup>. This means that industrial practical irradiated ion beams (irradiation energy of less than 5 MeV) can significantly improve the current-carrying capacity of 2G-HTS tapes in an external magnetic field at the appropriate radiation dose.

In 2021, Huang *et al.* irradiated YBCO/BTO nanocomposite films with low-energy protons at 60 keV and successfully introduced densely distributed small-sized (2-4 nm) defects, which combined with BTO precipitation (5-15 nm) in the YBCO/BTO nanocomposite film to form an effective mixed pinning landscape (as shown in Figure 8A)<sup>[108]</sup>. This hybrid pinning landscape can significantly improve the  $J_c$  of the

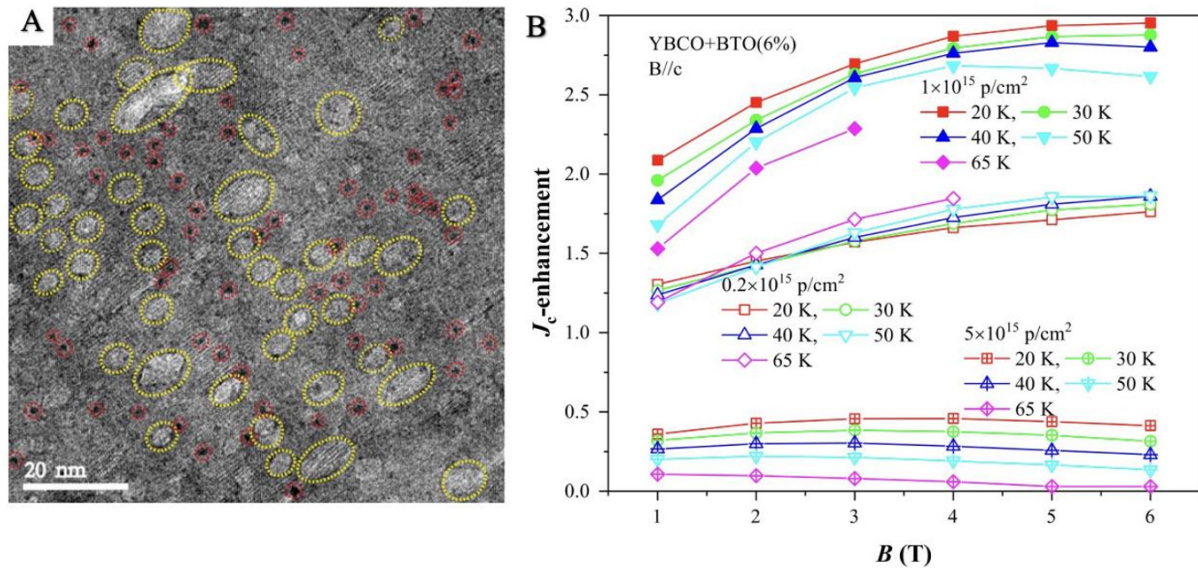


**Figure 8.** Microstructural characterization of irradiated YBCO/BZO nanocomposite films and the relationship between  $J_c$  and magnetic field. (A) Low-magnification microscope image of the sample when the irradiation dose is  $1 \times 10^{15}$  proton/cm<sup>2</sup>, in which the bright patches are BTO nanoparticles and the black spots are smaller irradiation defects. (B) Relationship between the enhancement factor of  $J_c$  and the magnetic field of YBCO/BTO nanocomposite films under different irradiation doses and temperatures<sup>[108]</sup> © 2021 IOP Publishing Ltd. Printed in the UK.

YBCO superconducting film under the conditions of low temperature and a strong magnetic field. As shown in Figure 8B, when the irradiation dose is  $1 \times 10^{15}$  protons/cm<sup>2</sup>, the  $J_c$  of the YBCO/BTO nanocomposite film increases nearly threefold (20 K, 6 T). Ion irradiation can produce nanocolumnar defects with an appropriate energy dose. This is an effective method to improve the flux pinning for ex-situ tapes, such as MOD and RCE, which lack 1D defects. In view of the improvement of ion irradiation on the magnetic transmission performance of 2G-HTS tapes, a roll-to-roll ion irradiation system established by the Brookhaven National Laboratory in the United States can irradiate tape products with a width of 45 mm and a length of 200 m, such as AMSC. It can double the magnetic field transmission performance of 2G-HTS tapes at the cost of \$1/m for irradiation<sup>[109,110]</sup>.

#### *Enhanced flux pinning through nano second-phase doping*

Nano second-phase doping mainly introduces a doped phase into a superconductor at the nanoscale to form impurity phases. The types of nano second-phase doping are plentiful, including the perovskite structure  $\text{BaMO}_3$  ( $M = \text{Zr, Hf or Sm}$ ), halogen elements, nanowires, and so on. The most representative is the doped  $\text{BaMO}_3$  perovskites, with BZO doping being particularly widely studied due to its good performance. A mismatch between the BZO and YBCO lattices can generate a lattice distortion field to improve the flux pinning. From the perspective of thermodynamics and dynamics, the nucleation and phase formation temperature of BZO is higher than that of the superconducting layer, so the growth rate of BZO is relatively slow and the particle size is small, which meets the small size requirement of APCs. The most crucial point is that Zr will not react with the superconducting layer so that it can avoid the destruction of the superconducting performance of the matrix.

In 2004, the first artificial pinning center of BZO was introduced into REBCO. MacManus-Driscoll *et al.* pioneered BZO doping into YBCO films and significantly improved their flux pinning<sup>[111]</sup>. Based on the low-cost MOD method, Gutierrez *et al.* prepared YBCO-BZO nanocomposite superconducting films with a randomly distributed orientation of BZO nanodots (as shown in Figure 9A and B)<sup>[112]</sup>. The angle-dependent

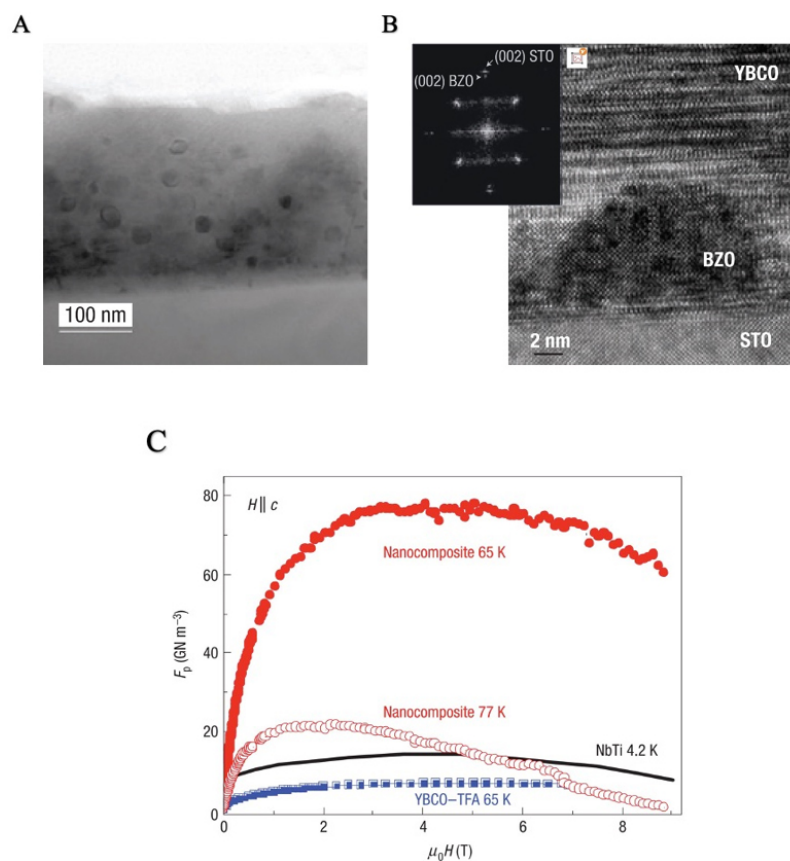


**Figure 9.** Microstructural characterization of YBCO/BZO nanocomposite films and the relationship between  $F_p$  and magnetic field. (A) Cross-sectional TEM image of the nanocomposite film along the  $\langle 100 \rangle$  direction of YBCO, which clearly shows the BZO nanodots. (B) High-resolution TEM image of BZO nanodots grown on a single-crystal substrate interface. The inset is a fast Fourier transformation image, where the diffraction peaks of BZO and YBCO show a mutual epitaxy relationship. (C) Compared with the standard YBCO-TFA film (65 K) and NbTi wire (4.2 K), the  $F_p$  curves of YBCO/BZO nanocomposite films at 65 and 77 K were obtained<sup>[112]</sup> © 2007 Nature Publishing Group.

critical current measurements show that the strongly isotropic flux pinning landscape is very efficient at high temperatures and magnetic fields. The YBCO/BZO films achieved a maximum vortex-pinning force ( $F_p$ ) of  $78 \text{ GNm}^{-3}$  at 65 K, 500% higher than the optimal value for NbTi superconductors at 4.2 K (a detailed comparison of the differences can be seen in Figure 9C). The enhanced pinning observed for all magnetic-field orientations derives from a high density of quasi-isotropic defects in the YBCO matrix strongly influenced by non-coherent BZO nanodots. The uniqueness of the defects in these films arises from a modified crystallization mechanism where non-coherent BZO nanodots remain trapped within the epitaxial films. Wang *et al.* prepared BZO-doped YBCO thin films with a particle size of  $\sim 5 \text{ nm}$  by the PLD method<sup>[113]</sup>. The  $J_c$  of the BZO-doped YBCO superconducting thin films reached 7.8, 26.5, and  $64.5 \text{ MA/cm}^2$  at 65, 40, and 5 K, respectively.

BZO-APCs are very effective in improving the performance of 2G-HTS tapes. In recent years, the doping of BZO nanorods has achieved excellent performance, among which the most representative is the high concentration Zr doping by Selvamanickan's team at the University of Houston. Unlike the RCE and MOD technology routes for the *ex situ* growth of superconducting layers, the in-situ PLD and MOCVD methods meet the kinetic and thermodynamic requirements for the growth of 1D columnar BZO nanorods. The RCE and MOD methods mainly grow into BZO nanoparticles. In 2015, the Selvamanickan team used the

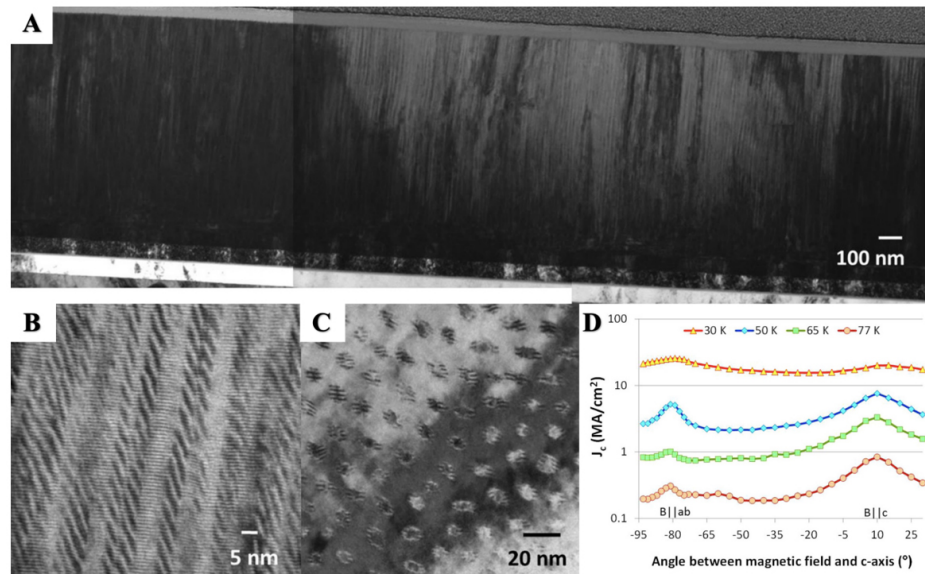


**Figure 10.** Microstructure and performance test diagram of 25% Zr-added (Gd, Y) BCO superconducting tape. (A and B) Cross-sectional TEM images. (C) Plan view TEM. (D) Angular dependence of  $J_c$  of this tape in a magnetic field of 3 T at 77, 65, 50, and 30 K<sup>[114]</sup> © 2015 AIP Publishing LLC.

MOCVD route to produce successfully (Gd, Y)Ba<sub>2</sub>Cu<sub>3</sub>O<sub>x</sub> superconductor tapes with a Zr-doping concentration of up to 25%<sup>[114]</sup>. According to the TEM images in Figure 10A-C, the BZO nanorods almost penetrate the entire superconducting layer and the diameter of the nanopillars is ~6 nm. In the previously reported PLD, MOD and MOCVD routes, the amount of Zr doping did not exceed 10%. They produced tapes three times higher than the typical doping level, with an  $I_c$  exceeding 20 MA/cm<sup>2</sup> (30 K, 3 T) and an  $F_p$  exceeding 1000 GN/m<sup>3</sup> at 20 K. Compared with the previous work from the team, the higher Zr content does not make the BZO nanorods thicker, but the density of the nanorods increases twice as much as that for 15% Zr doping<sup>[115]</sup>. The performance of the 2G-HTS tapes is greatly improved, especially the nearly isotropic current-carrying performance under 30 K and 3 T [Figure 10D]. The isotropic performance is mainly attributed to the BZO nanorods oriented along the c-axis for a higher  $J_c$  value of B//c-axis and randomly distributed isotropic defects.

The doping of BaHfO<sub>3</sub> (BHO) also yields a similar structure to that of BZO, effectively improving the performance of the tapes. Many other studies, using BHO-doped YBCO film (2016, Teranishi *et al.*<sup>[116]</sup>) and YGBCO film (2018, Liu *et al.*<sup>[117]</sup>), also achieved the same effect as above. Dong *et al.* fabricated BaMnO<sub>3</sub> (BMO)-doped YBCO nanocomposite films by a low-cost low-fluorine MOD route and reduced the BMO particle size ( $3 \pm 1$  nm) by controlling the heating rate in the mid-temperature stage<sup>[118]</sup>. The  $T_c$  of the obtained YBCO/BMO nanocomposite films decreased slightly, but the flux-pinning performance was improved.

In addition to the single-perovskite doping methods mentioned above, double-perovskite doping is also attractive, especially for high-field magnet applications. Celentano *et al.* explored the effect of growth rate on the microstructure and properties of mixed 2.5 mol.% BYTO and 2.5 mol.% BYNO double-perovskite secondary phase-doped YBCO nanocomposite films by the PLD method<sup>[119]</sup>. TEM analysis showed that when the deposition rate (R) of the composite film increased from 0.02 to 1.2 nm/s in the mixed composition of BYNO+BYTO (BYNTO), the microstructure of the composite film (BYNTO-YBCO) evolved from sparse straight columns to dense, thin and hashed continuous columns. When R = 0.3 nm/s,

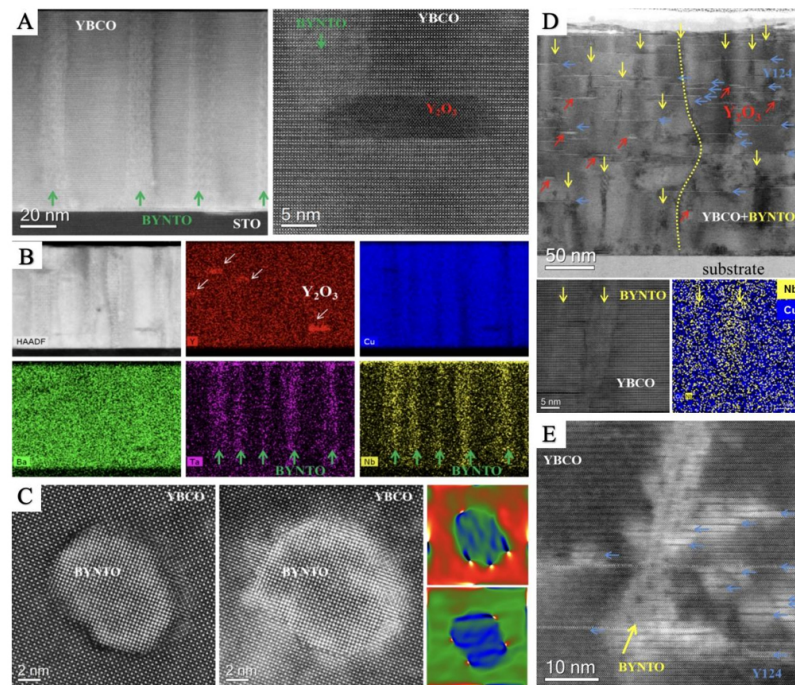


**Figure 11.** TEM investigations of BYNTO-YBCO films. (A) Cross-section view. The left half panel: an overview of the HAADF-STEM; the right half panel: a high-resolution HAADF STEM image. (B) Cross-section view: the HAADF STEM image shows the mapped area as well as the elemental Y, Ba, Cu, Ta, and Nb EDX maps. (C) Plan view. The left and center panels are HAADF and LAADF STEM Z-contrast images, and the right is GPA maps. (D) Top panel: an overview of ABF STEM. Bottom panel: High-resolution HAADF STEM image. (E) ADF STEM image showing the strain as brighter contrast features around the short Y124 intergrowths (blue arrows) and BYNTO nanocolumn<sup>[119]</sup> © ENEA Frascati Research Centre. Printed in the UK.

the nanocomposite films show excellent performance over the whole magnetic field and temperature ranges, with the maximum  $F_p$  reaching  $900 \text{ GN/m}^3$  (10 K, 12 T). When films are deposited at higher deposition rates (e.g.,  $R = 1.8 \text{ nm/s}$ ), BYNTO columns show sinuous properties and easily form short nanorods. Furthermore, a more disordered high-density short stacking-fault structure is observed in the YBCO matrix (the TEM image of the microstructure of the BYNTO-YBCO film is shown in Figure 11). At this time, the vortex pinning of the BYNTO-YBCO nanocomposite films is no longer controlled by the BYNTO columnar defects, but by a new mechanism with a typical temperature scaling law, as characterized by the significant  $J_c$  improvement at low temperature ( $F_p = 700 \text{ GN/m}^3$  at 10 K, 12 T, against  $F_p = 900 \text{ GN/m}^3$  at 4.2 K, 18 T). Gondo *et al.* also used the PLD method to prepare YBCO nanocomposite films doped with double-perovskite  $\text{Ba}_2\text{LuNbO}_6$  (BLNO)<sup>[120]</sup>. The BLNO-YBCO matrix has a mixed pinning landscape composed of Y-rich nanoparticles, BLNO nanorods, and stacking faults. BLNO forms self-assembled nanorods extending directly from the substrate to the surface in the YBCO films. The  $J_c$  value of the BLNO-YBCO thin films is larger than that of the traditional perovskite nanorod YBCO films under the action of a magnetic field.

Among the four methods mentioned above, nano second-phase doping in the superconducting layer is the most effective method to improve the current-carrying performance of 2G HTS tapes. It was found that an induced self-assembly 1D heterostructure by preferential growth in the c-axis direction can form a more effective flux pinning center. Particle irradiation is usually used in the post-treatment of superconducting thin films, which can accurately control the type, concentration, and angle of introduced defects. This suggests that REBCO tapes prepared under the optimal process conditions can further enhance their superconducting properties by particle irradiation.

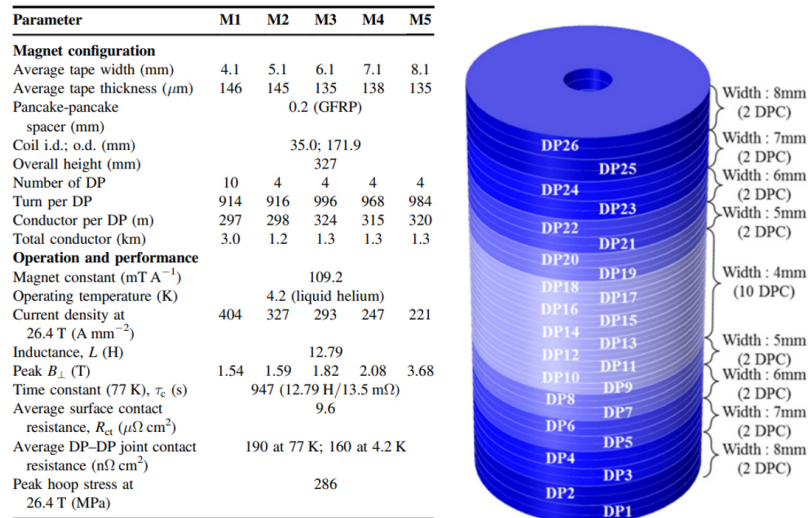


**Figure 12.** 26.4 T magnet parameters and structure diagram<sup>[124]</sup> © 2016 IOP Publishing Ltd. Printed in the UK.

## HIGH-TEMPERATURE SUPERCONDUCTING MAGNET BASED ON 2G-HTS TAPES

With the improvement of the performance of 2G-HTS tapes, a series of breakthroughs have been made in the development of superconducting magnets based on 2G-HTS tapes. SuNAM has developed an all-REBCO tape superconducting magnet with a magnetic field of 26.4 T. The IEECAS used REBCO insert magnets to achieve a 32.35 T all-superconducting magnet, setting a world record for an all-superconducting magnet. The NHMFL has developed a 45.5 T hybrid magnet using the insert magnet of 2G-HTS tapes. This broke the 19-year-old 45 T world record.

### Progress of all-2G-HTS tapes superconducting magnets

SuperPower manufactured an all-2G-HTS magnet in 2008. At 4.2 K, the magnet generated a 9.81 T self-field operating at a critical current of 221 A<sup>[121,122]</sup>. In addition, a large bore magnet coil wound without turn-to-turn insulation was fabricated by SuNAM in 2013. The assembled magnet was installed in a cryostat and tested up to 4.1 T at 10 K<sup>[123]</sup>.

In 2015, SuNAM and the Massachusetts Institute of Technology (MIT) jointly constructed all-2G-HTS tapes superconducting magnets with a cold hole diameter of 35 mm and produced a central field of 26.4 T at an operating current of 4.2 K, 242 A. This magnet was designed by the MIT Francis Bitter Magnet Laboratory and constructed and tested by the SuNAM Co., Ltd. The magnet consists of 26 uninsulated double pie coils, as shown in Figure 12<sup>[124]</sup>. This is the highest magnetic field record ever produced by an all-2G-HTS magnet. The test curve of the magnet at 4.2 K is shown in Figure 13. Meanwhile, SuNAM and the NHMFL designed a higher 35 T all-2G-HTS magnet in 2017<sup>[125]</sup>.

In 2018, after SuNAM manufactured the highest all-2G-HTS tape superconducting magnet, the IEECAS designed and manufactured an all-2G-HTS magnet with an inner diameter of 100 mm. At 4.6 K, the magnet generated a 4.08 T self-field operating at a critical current of 338 A<sup>[126]</sup>. It is noteworthy that SuNAM used tapes with different widths in winding REBCO superconducting magnets. Wider tapes are used in areas where the vertical field of the magnet is larger and narrower tapes are used in the central area. This method increases the safety margin of the magnet and improves the utilization rate of the tapes as much as possible.

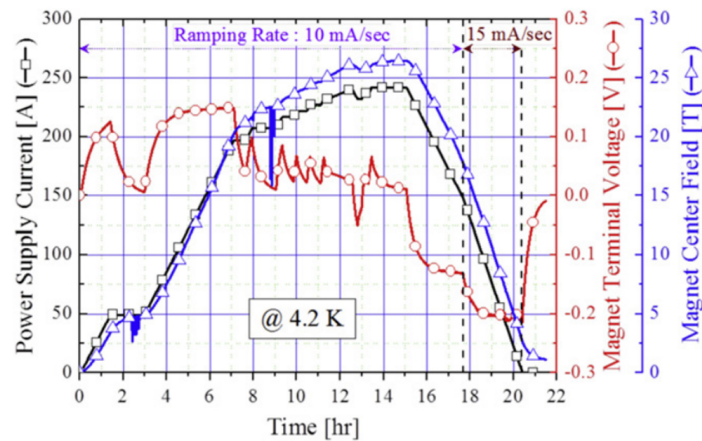


**Figure 13.** Test results in liquid helium at 4.2 K. Ramping was occasionally halted to check the magnet status. The axial field mapping was completed at a power supply current of 207 A. The magnet reached 26.4 T at a power supply current of 242 A<sup>[124]</sup> © 2016 IOP Publishing Ltd. Printed in the UK.

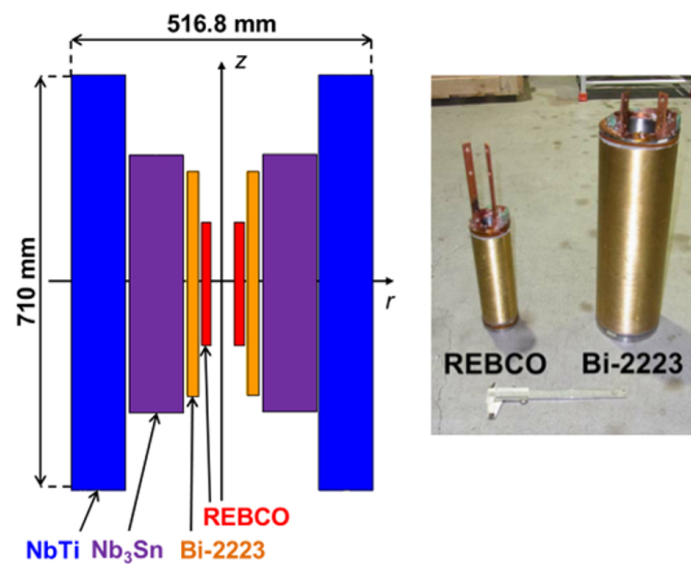


**Figure 14.** Cross section of the magnet with the REBCO coil, the Bi-2223 coil, the Nb<sub>3</sub>Sn coils and the NbTi coils<sup>[127]</sup> 1051-8223 © 2016 IEEE.

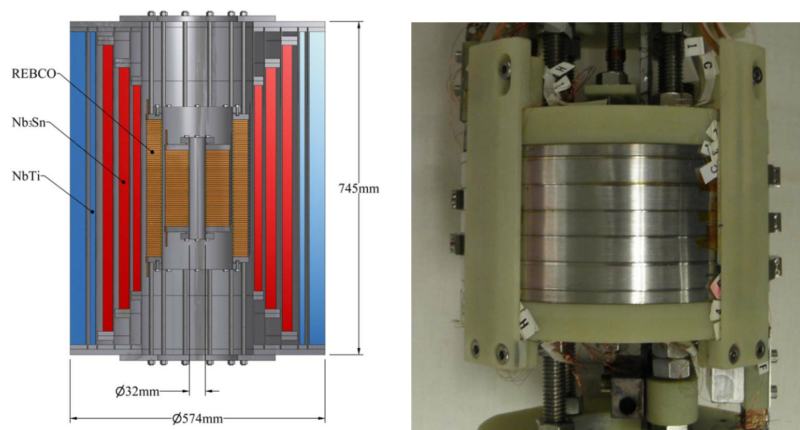
### Progress of all-superconducting magnets

In 2016, REKIN conducted a test experiment when manufacturing NMR magnets and designed a 28 T all-superconducting magnet by layer winding<sup>[127]</sup>. As shown in Figure 14 and Table 3, the magnet comprises 17 T LTS and 11 T HTS, and the insert magnet is composed of REBCO and Bi2223 coils. Without a background field, the central magnetic field reaches 25 T and the REBCO tape has a delamination phenomenon.

To change the delamination, RIKEN connected the welded joints to the flanges. There were no joints inside the coils and the outermost layer of the coils was bound and thickened to obtain an all-superconducting magnet with a central magnetic field of 27.6 T<sup>[128]</sup>.

**Table 3. Superconducting magnet parameters of 28.2 T<sup>[127]</sup>**

Parameters	REBCO coil	Bi2223 coil	LTS coils
Conductor manufacturer	Fujikura	SEI	JASTEC
Winding method	Layer-winding	Layer-winding	-
Coil inner diameter (mm)	40	81	135
Coil outer diameter (mm)	71.68	123.66	517
Coil height (mm)	210	384	710
Number of total turns	3700	4640	-
Self-inductance (H)	0.15	0.45	-
Operating current (A)	304.9	304.9	241.1
Current density in the conductor ( $A/mm^2$ )	412.0	221.0	-
Central magnetic field (T)	6.52	4.47	17.2

**Figure 15.** 32 T magnet structure and REBCO test coil consisting of six double-pancake modules<sup>[129]</sup> 1051-8223/\$26.00 © 2011 IEEE.

The NHMFL manufactured a high and low-temperature all-superconducting hybrid magnet with a hole diameter of 32 mm in 2017, with its center field strength reaching 32 T [Figure 15]. The two outer NbTi coils and the middle three Nb<sub>3</sub>Sn coils provide a 15 T background field for the insert HTS magnet, and the insert magnet wound with 2G-HTS tapes contributes a center field of 17 T at the temperature of liquid helium<sup>[129]</sup>.

In 2016, the IEECAS increased the central magnetic field of the YBCO insert magnet to 24 T (4.2 K) under a 15 T superconducting backfield. Later, the IEECAS developed a high-field insert magnet using YBCO tapes. When the operating current of the insert magnet is 32 A under the liquid nitrogen test conditions, the center magnet reaches 1.62 T (77 K). At the liquid-helium test conditions, when the operating current of the insert magnet of 167 A, it generates a 9 T central magnetic field in the 15 T superconducting backfield, thus realizing an all-superconducting magnet with a central field of 24 T and a highest field of 24.3 T<sup>[130,131]</sup>.

In 2020, the IEECAS designed and manufactured a 12 T insert magnet for 27 T all-superconducting magnets. The structure is shown in Figure 16. A 12 T insert magnet is constructed in a 15 T LTS magnet, and finally a magnetic field with a field strength of 27.2 T is obtained at a current of 169 A. The 12 T insert magnet was placed in a 15 T background field and tested at liquid helium temperature. For the power supply current, the ramping rate was first 50 mA/s from 0 to 100 A and then decreased from 4 to 2 mA/s. When the central magnetic field reached 26.55 T, the power supply current was kept at 160 A for 2 h. They

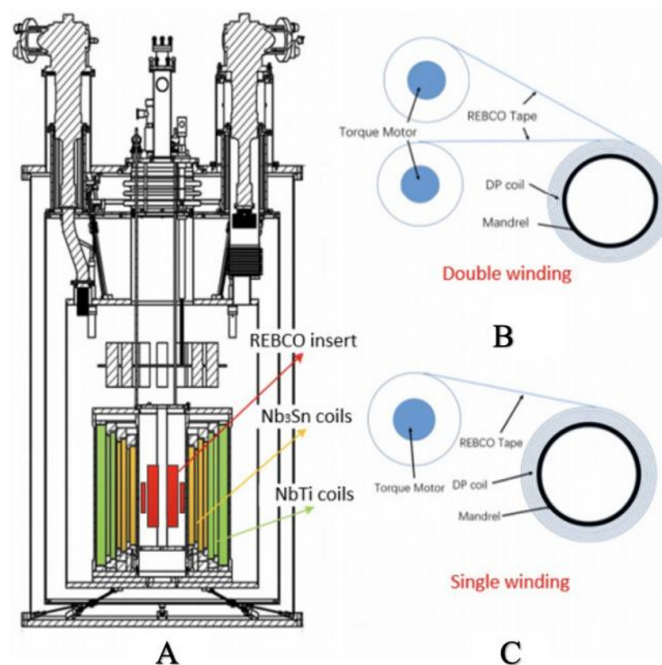


**Figure 16.** (A) Designed 27 T magnet system. (B) Double-winding method. (C) Single-winding method<sup>[132]</sup> 1051-8223 © 2020 IEEE.

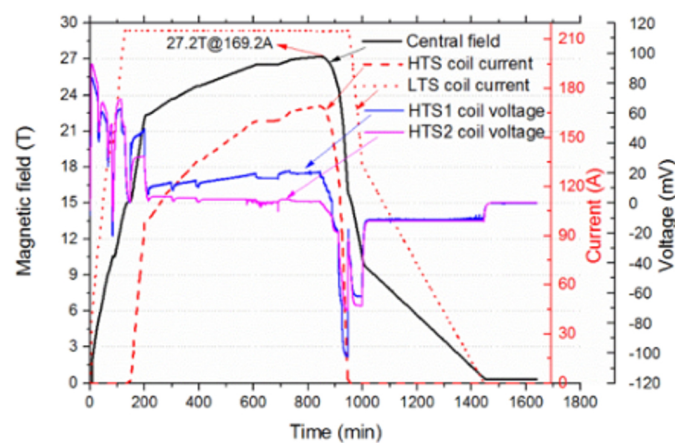


**Figure 17.** Test of REBCO insert magnets under 15 T background magnetic field at 4.2 K<sup>[132]</sup> 1051-8223 © 2020 IEEE.

then increased the power supply current to 169.2 A at a ramping rate of 0.5 mA/s. Finally, a central magnetic field of 27.2 T was obtained [Figure 17]<sup>[132]</sup>.

In 2020, subsequently, the all-superconducting magnets of the IEECAS successfully reached the world record of a 32.35 T DC magnetic field. The magnet consists of a 15 T low-temperature superconductor outer coil and two high-temperature superconductor no-insulation insert coils using a conductor tape coated with REBCO, as shown in Figure 18<sup>[133]</sup>. This is the highest field of all-superconducting magnets that have been achieved, which reflects the superiority of 2G-HTS tapes in manufacturing high-field magnets. The test result is shown in Figure 19. In 2021, Suetomi *et al.* designed a 31.4 T LTS/Bi-2223/REBCO demo-magnet with a layer-wound REBCO inner coil, which is mainly intended for 1.3 GHz NMR<sup>[134]</sup>.

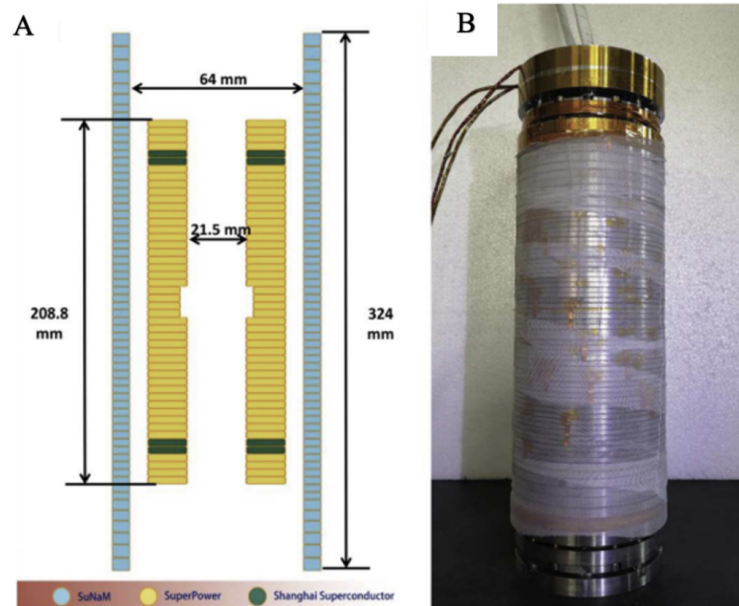


**Figure 18.** Design and construction of REBCO insert coil<sup>[133]</sup> © 2020 IOP Publishing Ltd. Printed in the UK.

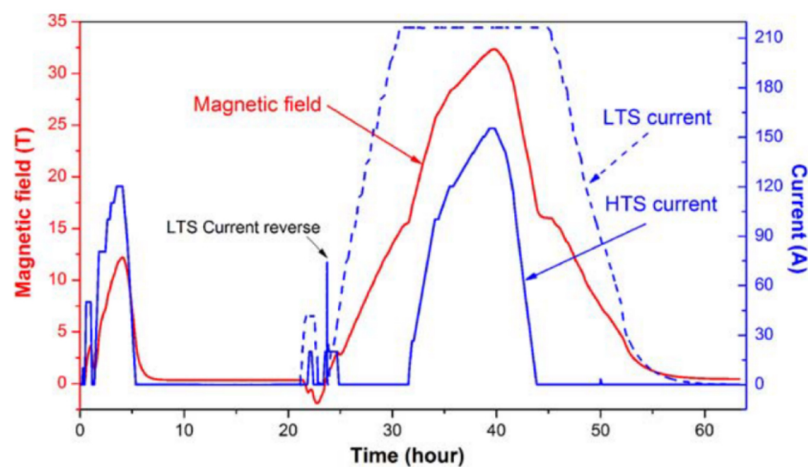


**Figure 19.** Test of REBCO insert under 15 T background magnetic field at 4.2 K<sup>[133]</sup> © 2020 IOP Publishing Ltd. Printed in the UK.

### Progress of hybrid insert magnets for 2G-HTS tapes

The NHMFL used a mixture of a 14 T high-temperature superconducting insert magnet and 31 T resistive magnets to obtain a steady-state magnet with a central magnetic field of 45 T<sup>[135]</sup>. In recent years, the NHMFL has also continued to hit the world record for higher magnetic fields. In 2019, NHMFL used REBCO coils as an insert magnet to create the highest direct-current magnetic field that can currently achieve 45.5 T<sup>[136]</sup>. The insert magnet [Figure 20] consists of a stack of 12 single pancake coils wound with REBCO tapes. Among them, the most innovative work is to use an ultrathin substrate, so that more turns can be incorporated in a limited space, thereby generating a higher magnetic field. This REBCO insert magnet uses a no-insulated winding scheme. When the magnetic field is too high and the magnet is partially quenched, the current can be bypassed through the nearby tapes. The no-insulation winding method can effectively avoid the burnout caused by the partial quench of the magnet. Due to the thinness of the chosen YBCO baseband, the interposer magnet has a very high current density. When the current reaches 245.3 A,

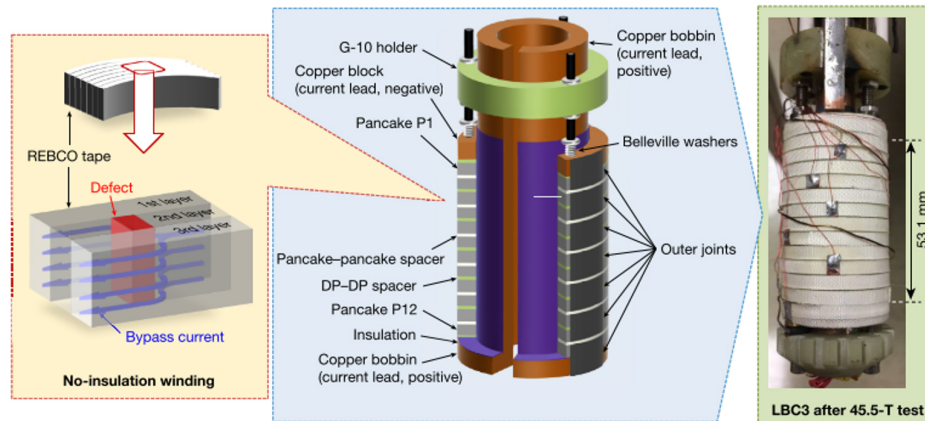


**Figure 20.** No insulation winding and REBCO insert magnet structure<sup>[136]</sup> © The Author(s), under exclusive license to Springer Nature Limited 2019.

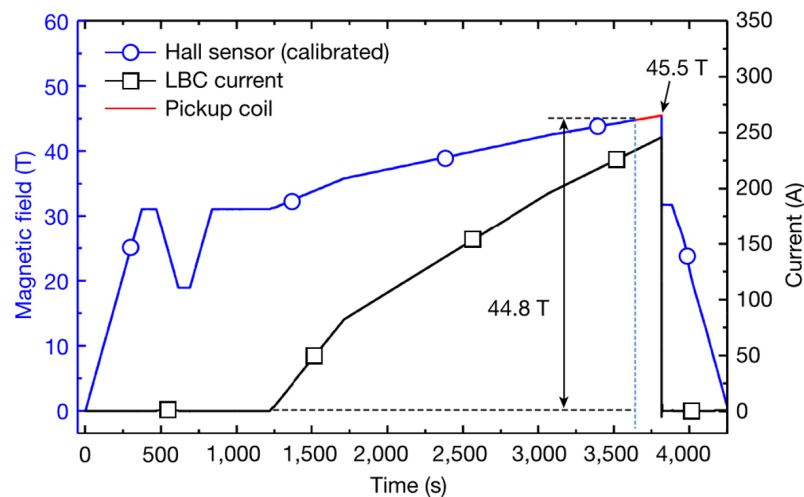


**Figure 21.** Magnet center magnetic field and test current<sup>[136]</sup> © The Author(s), under exclusive license to Springer Nature Limited 2019.

the magnetic field reaches 45.5 T [Figure 21] and the current density is up to 1420 A mm<sup>-2</sup>.

Notably, the NHMFL magnet was subjected to strong electromagnetic stress during the interpolated magnet testing, which resulted in cracks at the edges of the REBCO tapes. Post-mortem analysis of the superconducting tape showed that the damage was caused by the cutting edge of the tape facing the direction of force after cutting the 12 mm wide tape into 4 mm. The NHMFL reported that the proper placement of the single pancake coils with the insert magnets in the background magnetic field can be used to avoid tape damage and hopefully generate a higher magnetic field of > 45.5 T<sup>[136]</sup>.

### Difficulties and challenges of 2G-HTS tapes in high magnetic field applications

In the application of high magnetic fields, 2G-HTS tapes mainly suffer from the problems of delamination, a lack of early quench detection technique, anisotropy, and a sharp current-carrying capacity drop at high temperature (77 K) with increasing external magnetic field strength. We need to pay attention to the layered structure and multi-layer packaging of 2G-HTS tapes, which are prone to interlayer separation or tearing in high fields. In the coil winding and magnet structure design, a large number of practical technologies have

been developed in order to avoid the delamination of 2G-HTS tapes. For example, double-cake winding, non-insulating winding, multi-width winding, and other schemes greatly improve the performance and stability of the magnet. Excessive stress release or electromagnetic force in part of the coils will cause the coils or part of the tapes to be torn or arched and deformed<sup>[137]</sup>.

2G-HTS tapes may quench during magnet operation due to localized conductor degradation or excessive temperature at a certain point. The lack of effective quench detection methods is a challenge for the construction of extremely high-field magnets with 2G-HTS tapes. At present, the quench detection technology of HTS magnets is still in the exploratory stage based on the detection technology of LTS magnets. The problems faced by HTS magnet quench detection mainly include the existence of lag time in the detection voltage signal, difficulty in detecting weak voltage signals after quench, and the lack of theoretical model analysis and quench experimental data for large HTS magnets<sup>[138,139]</sup>.

2G-HTS tapes are reproduced in tape form with a wide aspect ratio, which is limited in applications where isotropic tapes are preferred. To reduce anisotropy, REBCO tapes can be converted to various formats, including round wires<sup>[140]</sup>. Round superconducting wires can make the current distribution more uniform and current-sharing to circumvent possible defective regions in a strand. However, the REBCO superconductor will suffer more severe strains due to the twisted shape of the round wire. In addition to this, the performance of round wire wound magnets is closely related to the minimum bending radius of the 2G-HTS tapes<sup>[141]</sup>. If the bending radius of the tapes is larger, a large inclination angle must be used when winding the round wire, which limits the generation of higher magnetic fields<sup>[140]</sup>.

When 2G-HTS tapes are in the high-temperature range (77 K), with increasing external magnetic field strength, the current-carrying capacity drops sharply, which restricts the application of 2G-HTS magnets in the high-temperature range. The University of Houston has effectively improved the field performance of 2G-HTS tapes through high-density Zr doping and achieved a significant increase in the current-carrying capacity at 77 K.

### **Cost performance and market competitiveness of 2G-HTS tapes**

The cost performance and market acceptance of 2G-HTS tapes are also challenging issues. With the exception of some particular application scenarios, HTS materials have always been compared and competed with traditional superconductors and metal conductors in terms of cost performance. The prices of 2G-HTS tapes have continued to decrease over the years. Five years ago, the price of 2G-HTS tapes was in the range of \$300-500/K·A·m. At present, the market price of 2G-HTS tapes is still in the range of \$100-150/K·A·m, which is three to four times higher than the price of copper<sup>[142]</sup>. This is five to eight times lower than the price of ten years ago. However, the cost of 2G-HTS tapes is still relatively high, thereby limiting their application. In addition to factors such as low temperature and operating costs, only the cost performance of 2G-HTS tapes has significantly improved (e.g., \$25-50/KA·m). When the cost performance of 2G-HTS tapes reaches the equivalent of copper, it is possible to gain widespread acceptance and large-scale application. Therefore, to improve the cost-effectiveness of 2G-HTS tapes and promote more market applications, researchers must further enhance the current-carrying performance, production efficiency and yield of 2G-HTS finished tapes<sup>[143-148]</sup> and excavate existing technologies while exploring new component structures, technical routes, or transformative technologies.

## **CONCLUSION AND OUTLOOK**

Various new superconducting materials will continue to emerge in the future. However, in terms of applications, technical indicators, such as the intrinsic properties of 2G-HTS tapes and the high irreversible

field in the liquid nitrogen temperature region, still have comprehensive advantages. From the perspective of economics and engineering applications, 2G-HTS tapes have more potential for development. Therefore, the preparation of high-performance, low-cost and long 2G-HTS tapes is the direction of various efforts globally. At present, the preparation technology of 2G-HTS tapes has made significant progress, and companies all over the world have the ability to supply small quantities. In recent years, continuous progress has been made in improving the performance of 2G-HTS tapes, especially in the development of nanoscale APCs, which has laid the foundation for further enhancing the performance of 2G-HTS tapes in a wider magnetic field and temperature ranges.

The high field electromagnetic environment plays a critical role in the development of science and technology and is widely used in physics, chemistry, materials science, and life sciences. Since the discovery of 2G-HTS tapes, significant progress has been made in high field applications, and some large scientific installations are all carried out to obtain high field electromagnetic environments. For the development of ultra-high magnetic field magnets, 2G-HTS tapes are a suitable choice, which are expected to get a higher and more stable magnetic field, which will significantly promote scientific research in condensed-matter physics, chemistry, materials science, and life sciences.

## **DECLARATIONS**

### **Authors' contributions**

Designed and wrote the original draft: Wang K, Dong H

Reviewed and revised the manuscript: Gu H, Ding F

References search: Huang D, Shang H, Xie B

Manuscript layout: Zou Q, Zhang L, Feng C

### **Availability of data and materials**

Not applicable.

### **Financial support and sponsorship**

This work was supported by the National Key R&D Program of China (Grant No. 2022YFE03150200), the National Natural Science Foundation of China (Grant No. U2032217, Grant No. 52072366, and Grant No. 51721005), the Beijing Natural Science Foundation (Grant No. 3202034), the Dalian National Laboratory for Clean Energy (DNL), CAS, DNL Cooperation Fund, CAS(DNL202021), the Youth Innovation Promotion Association of the Chinese Academy of Sciences (Y202041), and China Postdoctoral Science Foundation (Grant No. 2021M703198).

### **Conflicts of interest**

All authors declared that there are no conflicts of interest.

### **Ethical approval and consent to participate**

Not applicable.

### **Consent for publication**

Not applicable.

### **Copyright**

© The Author(s) 2022.

## REFERENCES

1. Onnes HK. Further experiments with liquid helium, C - On the change of electric resistance of pure metals at very low temperatures etc IV - The resistance of pure mercury at helium temperatures. The Amsterdam: Koninklijke Akademie Van Wetenschappen Te Amsterdam; 1910. p. 1274-6. [DOI](#)
2. Onnes HK. Further experiments with liquid helium D - On the change of the electrical resistance of pure metals at very low temperatures, etc V - The disappearance of the resistance of mercury. The Amsterdam: Koninklijke Akademie Van Wetenschappen Te Amsterdam; 1911. p. 113-5. [DOI](#)
3. Meissner W, Ochsenfeld R. Ein neuer Effekt bei Eintritt der Supraleitfähigkeit. *Naturwissenschaften* 1933;21:787-8. [DOI](#)
4. Josephson B. Possible new effects in superconductive tunnelling. *Phys Lett* 1962;1:251-3. [DOI](#)
5. Petley BW. The Josephson effects. *Contemp Phys* 1969;10:139-58. [DOI](#)
6. Mooij JE, Orlando TP, Levitov L, Tian L, van der Wal CH, Lloyd S. Josephson persistent-current qubit. *Science* 1999;285:1036-9. [DOI](#) [PubMed](#)
7. Bardeen J, Cooper LN, Schrieffer JR. Theory of Superconductivity. *Phys Rev* 1957;108:1175-204. [DOI](#)
8. Abrikosov AA. On the magnetic properties of superconductors of the second group. *Soviet Physics JETP-USSR* 1957;5:1174-83.
9. Bednorz JG, Müller KA. Possible high-T<sub>c</sub> superconductivity in the Ba-La-Cu-O system. *Condens Matter* 1986;64:189-93. [DOI](#)
10. Wu MK, Ashburn JR, Torng CJ, et al. Superconductivity at 93 K in a new mixed-phase Yb-Ba-Cu-O compound system at ambient pressure. *Phys Rev Lett* 1987;58:908-10. [DOI](#) [PubMed](#)
11. Zhao Z X, Chen L Q, Yang Q S, et al. Superconductivity above liquid-nitrogen temperature in new oxide systems. *Kexue Tongbao* 1987;32:1098-102. [DOI](#)
12. Maeda H, Tanaka Y, Fukutomi M, Asano T. A new high-T<sub>c</sub> oxide superconductor without a rare earth element. *Jpn J Appl Phys* 1988;27:L209-10. [DOI](#)
13. Ayai N, Hayashi K, Yasuda K. Development of Bi-2223 superconducting wires for AC applications. *IEEE Trans Appl Supercond* 2005;15:2510-3. [DOI](#)
14. Scanlan R, Malozemoff A, Larbalestier D. Superconducting materials for large scale applications. *Proc IEEE* 2004;92:1639-54. [DOI](#) [PubMed](#) [PMC](#)
15. Larbalestier D, Gurevich A, Feldmann DM, Polyanskii A. High-T<sub>c</sub> superconducting materials for electric power applications. *Nature* 2001;414:368-77. [DOI](#) [PubMed](#)
16. Choi SM, Lee JW, Shin GH, et al. Characteristics of high-J<sub>c</sub> GdBCO coated conductors fabricated by the RCE-DR process. *IEEE Trans Appl Supercond* 2013;23:8001004. [DOI](#)
17. Nagamatsu J, Nakagawa N, Muranaka T, Zenitani Y, Akimitsu J. Superconductivity at 39 K in magnesium diboride. *Nature* 2001;410:63-4. [DOI](#) [PubMed](#)
18. Buzea C, Yamashita T. Review of the superconducting properties of MgB<sub>2</sub>. *Supercond Sci Technol* 2001;14:R115-46. [DOI](#)
19. Kortus J, Mazin II, Belashchenko KD, Antropov VP, Boyer LL. Superconductivity of metallic boron in MgB<sub>2</sub>. *Phys Rev Lett* 2001;86:4656-9. [DOI](#) [PubMed](#)
20. Kamihara Y, Watanabe T, Hirano M, Hosono H. Iron-based layered superconductor La[O(1-x)F(x)]FeAs (x = 0.05-0.12) with T<sub>c</sub> = 26 K. *J Am Chem Soc* 2008;130:3296-7. [DOI](#) [PubMed](#)
21. Wen H, Mu G, Fang L, Yang H, Zhu X. Superconductivity at 25 K in hole-doped (La<sub>1-x</sub>Sr<sub>x</sub>)OFeAs. *Europhys Lett* 2008;82:17009. [DOI](#)
22. Sasmal K, Lv B, Lorenz B, et al. Superconducting Fe-based compounds (A<sub>1-x</sub>Sr<sub>x</sub>)Fe<sub>2</sub>As<sub>2</sub> with A=K and Cs with transition temperatures up to 37 K. *Phys Rev Lett* 2008;101:107007. [DOI](#) [PubMed](#)
23. Mai ZH, Chen LQ, Chu X, et al. The identification of 2 superconducting phases in the Tl-Ba-Ca-Cu oxide system. *Superconduct Sci Technol* 1988;1:94-6. [DOI](#)
24. Eggert JH, Hu JZ, Mao HK, Beauvais L, Meng RL, Chu CW. Compressibility of the HgBa<sub>2</sub>C<sub>an</sub>-1C<sub>un</sub>O<sub>2n+2</sub>+ $\delta$  (n = 1,2,3) high-temperature superconductors. *Phys Rev B Condens Matter* 1994;49:15299-304. [DOI](#) [PubMed](#)
25. Nuñez-Regueiro M, Tholence JL, Antipov EV, Capponi JJ, Marezio M. Pressure-induced enhancement of T<sub>c</sub> above 150 K in Hg-1223. *Science* 1993;262:97-9. [DOI](#) [PubMed](#)
26. Crisan A. Vortices and nanostructured superconductors. Cham: Springer; 2017. p. 1-259. [DOI](#) [PubMed](#)
27. Malozemoff AP, Fleshler S, Rupich M, et al. Progress in high temperature superconductor coated conductors and their applications. *Supercond Sci Technol* 2008;21:034005. [DOI](#)
28. Rupich MW, Verebelyi DT, Zhang W, Kodenkandath T, Li X. Metalorganic deposition of YBCO films for second-generation high-temperature superconductor wires. *MRS Bull* 2004;29:572-8. [DOI](#)
29. Lee S, Petrykin V, Molodyk A, et al. Development and production of second generation high T<sub>c</sub> superconducting tapes at SuperOx and first tests of model cables. *Supercond Sci Technol* 2014;27:044022. [DOI](#)
30. Selvamanickam V, Chen Y, Xiong X, et al. Recent progress in second-generation HTS conductor scale-up at superpower. *IEEE Trans Appl Supercond* 2007;17:3231-4. [DOI](#)
31. Selvamanickam V, Chen Y, Kesgin I, et al. Progress in performance improvement and new research areas for cost reduction of 2G HTS wires. *IEEE Trans Appl Supercond* 2011;21:3049-54. [DOI](#)
32. Zhao Y, Zhu J, Jiang G, et al. Progress in fabrication of second generation high temperature superconducting tape at Shanghai

- Superconductor Technology. *Supercond Sci Technol* 2019;32:044004. DOI
33. Yi-yuan Xie, Marchevsky M, Xun Zhang, et al. Second-generation HTS conductor design and engineering for electrical power applications. *IEEE Trans Appl Supercond* 2009;19:3009-13. DOI
  34. Yokoyama S, Miura H, Matsuda T, et al. Design and cooling properties of high stable field REBCO superconducting magnet for MRI. *IEEE Trans Appl Supercond* 2020;30:1-4. DOI
  35. Feighan JPF, Kursumovic A, Macmanus-driscoll JL. Materials design for artificial pinning centres in superconductor PLD coated conductors. *Supercond Sci Technol* 2017;30:123001. DOI
  36. Siegrist T, Sunshine S, Murphy DW, Cava RJ, Zahurak SM. Crystal structure of the high-Tc superconductor Ba<sub>2</sub>YCu<sub>3</sub>O<sub>9-δ</sub>. *Phys Rev B Condens Matter* 1987;35:7137-9. DOI PubMed
  37. Calestani G, Rizzoli C. Crystal structure of the YBa<sub>2</sub>Cu<sub>3</sub>O<sub>7</sub> superconductor by single-crystal X-ray diffraction. *Nature* 1987;328:606-7. DOI
  38. Mei Y, Green SM, Reynolds GG, Wiczynski T, Luo HL, Politis C. Magnetic properties of GdBa<sub>2</sub>Cu<sub>3</sub>O<sub>7-x</sub> in the normal and superconducting states. *Condensed Matter* 1987;67:303-5. DOI
  39. Jasiolek G, Niculescu H, Pajaczkowska A. XES studies of YBa<sub>2</sub>Cu<sub>3</sub>O<sub>y</sub> and GdBa<sub>2</sub>Cu<sub>3</sub>O<sub>y</sub>, single crystals. *Physica C Superconductivity* 1988;153-155:137-8. DOI
  40. Hull J, Murakami M. Applications of bulk high-temperature Superconductors. *Proc IEEE* 2004;92:1705-18. DOI
  41. Fleshler S, Buczek D, Carter B, et al. Scale-up of 2G wire manufacturing at American Superconductor Corporation. *Physica C Superconductivity* 2009;469:1316-21. DOI
  42. Iijima Y, Onabe K, Futaki N, et al. Structural and transport properties of biaxially aligned YBa<sub>2</sub>Cu<sub>3</sub>O<sub>7-x</sub> films on polycrystalline Ni-based alloy with ion-beam-modified buffer layers. *J Appl Phys* 1993;74:1905-11. DOI
  43. Goyal A, Norton D, Christen D, et al. Epitaxial superconductors on rolling-assisted biaxially-textured substrates (RABiTS): a route towards high critical current density wire. *Appl Superconduct* 1996;4:403-27. DOI
  44. Goyal A, Lee D, List F, et al. Recent progress in the fabrication of high-Jc tapes by epitaxial deposition of YBCO on RABiTS. *Physica C Superconductivity* 2001;357-360:903-13. DOI
  45. Rupich M, Schoop U, Verebelyi D, et al. YBCO coated conductors by an MOD/RABiTS/spl trade/ process. *IEEE Trans Appl Supercond* 2003;13:2458-61. DOI
  46. Goyal A, Paranthaman MP, Schoop U. The RABiTS approach: using rolling-assisted biaxially textured substrates for high-performance YBCO superconductors. *MRS Bull* 2004;29:552-61. DOI
  47. Wu XD, Foltyn SR, Arendt P, et al. High current YBa<sub>2</sub>Cu<sub>3</sub>O<sub>7-δ</sub> thick films on flexible nickel substrates with textured buffer layers. *Appl Phys Lett* 1994;65:1961-3. DOI
  48. Wang CP, Do KB, Beasley MR, Geballe TH, Hammond RH. Deposition of in-plane textured MgO on amorphous Si<sub>3</sub>N<sub>4</sub> substrates by ion-beam-assisted deposition and comparisons with ion-beam-assisted deposited yttria-stabilized-zirconia. *Appl Phys Lett* 1997;71:2955-7. DOI
  49. Arendt PN, Foltyn SR. Biaxially textured IBAD-MgO templates for YBCO-coated conductors. *MRS Bull* 2004;29:543-50. DOI
  50. Obradors X, Puig T, Pomar A, et al. Progress towards all-chemical superconducting YBa<sub>2</sub>Cu<sub>3</sub>O<sub>7</sub>-coated conductors. *Supercond Sci Technol* 2006;19:S13-26. DOI
  51. Hasegawa K, Fujino K, Mukai H, et al. Biaxially aligned YBCO film tapes fabricated by all pulsed laser deposition. *Appl Superconductivity* 1996;4:487-93. DOI
  52. Bauer M, Semerad R, Kinder H. YBCO films on metal substrates with biaxially aligned MgO buffer layers. *IEEE Trans Appl Supercond* 1999;9:1502-5. DOI
  53. Iijima Y, Tanabe N, Kohno O, Ikeno Y. In-plane aligned YBa<sub>2</sub>Cu<sub>3</sub>O<sub>7-x</sub> thin films deposited on polycrystalline metallic substrates. *Appl Phys Lett* 1992;60:769-71. DOI
  54. Goyal A, Norton DP, Budai JD, et al. High critical current density superconducting tapes by epitaxial deposition of YBa<sub>2</sub>Cu<sub>3</sub>O<sub>x</sub> thick films on biaxially textured metals. *Appl Phys Lett* 1996;69:1795-7. DOI
  55. Prusseit W, Nemetschek R, Hoffmann C, Sigl G, Lumkemann A, Kinder H. ISD process development for coated conductors. *Phys C Superconduct Appl* 2005;426-431:866-71. DOI
  56. Aabdin Z, Dürrschnabel M, Bauer M, Semerad R, Prusseit W, Eibl O. Growth behavior of superconducting DyBa<sub>2</sub>Cu<sub>3</sub>O<sub>7-x</sub> thin films deposited by inclined substrate deposition for coated conductors. *Acta Materialia* 2012;60:6592-600. DOI
  57. Zeng J, Ignatiev A, Zhou Y, Salama K. A single oxide buffer layer on a cube-textured Ni substrate for the development of YBCO coated conductors by photo-assisted MOCVD. *Supercond Sci Technol* 2006;19:772-6. DOI
  58. Holesinger T, Foltyn S, Arendt P, et al. A comparison of buffer layer architectures on continuously processed YBCO coated conductors based on the IBAD YSZ process. *IEEE Trans Appl Supercond* 2001;11:3359-64. DOI
  59. Wang SS, Han Z, Schmidt W, et al. Chemical solution growth of CeO<sub>2</sub> buffer and YBCO layers on IBAD-YSZ/Hastelloy templates. *Supercond Sci Technol* 2005;18:1468-72. DOI
  60. Xiong J, Tao BW, Qin WF, Tang JL, Han X, Li YR. Reel-to-reel continuous simultaneous double-sided deposition of highly textured CeO<sub>2</sub> templates for YBa<sub>2</sub>Cu<sub>3</sub>O<sub>7-δ</sub> coated conductors. *Supercond Sci Technol* 2008;21:025016. DOI
  61. Huhne R, Selbmann D, Eickemeyer J, Hänisch J, Holzapfel B. Preparation of buffer layer architectures for YBa<sub>2</sub>Cu<sub>3</sub>O<sub>7-x</sub> coated conductors based on surface oxidized Ni tapes. *Supercond Sci Technol* 2006;19:169-74. DOI
  62. Cai C, Yang Z, Guo Y, et al. The new power transmission material-REBaCuO high-temperature superconducting coated conductor. *Phys*

- Lett* 2020;49:747-54. DOI
63. Selvamanickam V, Chen Y, Xiong X, et al. High performance 2G wires: from R&D to pilot-scale manufacturing. *IEEE Trans Appl Supercond* 2009;19:3225-30. DOI
  64. Selvamanickam V, Chen Y, Xiong X, et al. Progress in second-generation HTS wire development and manufacturing. *Phys C Supercond* 2008;468:1504-9. DOI
  65. Lee J, Lee H, Lee J, Choi S, Yoo S, Moon S. RCE-DR, a novel process for coated conductor fabrication with high performance. *Supercond Sci Technol* 2014;27:044018. DOI
  66. Kim T, Lee J, Lee Y, Moon S. Development of an RGB color analysis method for controlling uniformity in a long-length GdBCO coated conductor. *Supercond Sci Technol* 2015;28:124006. DOI
  67. Rupich MW, Li X, Thieme C, et al. Advances in second generation high temperature superconducting wire manufacturing and R&D at American Superconductor Corporation. *Supercond Sci Technol* 2010;23:014015. DOI
  68. Shiohara Y, Taneda T, Yoshizumi M. Overview of materials and power applications of coated conductors project. *Jpn J Appl Phys* 2012;51:010007. DOI
  69. Tsuchiya K, Kikuchi A, Terashima A, et al. Critical current measurement of commercial REBCO conductors at 4.2 K. *Cryogenics* 2017;85:1-7. DOI
  70. Weiss JD, van der Laan DC, Hazelton D, et al. Introduction of the next generation of CORC® wires with engineering current density exceeding 650 A mm<sup>-2</sup> at 12 T based on SuperPower's ReBCO tapes containing substrates of 25 μm thickness. *Supercond Sci Technol* 2020;33:044001. DOI
  71. Tsuchiya K, Wang X, Fujita S, et al. Superconducting properties of commercial REBCO-coated conductors with artificial pinning centers. *Supercond Sci Technol* 2021;34:105005. DOI
  72. Usoskin A, Betz U, Gnisen J, Noll-baumann S, Schlenga K. Long-length YBCO coated conductors for ultra-high field applications: gaining engineering current density via pulsed laser deposition/alternating beam-assisted deposition route. *Supercond Sci Technol* 2019;32:094005. DOI
  73. Jiang G, Zhao Y, Zhu J, et al. Recent development and mass production of high J<sub>c</sub> 2G-HTS tapes by using thin hastelloy substrate at Shanghai Superconductor Technology. *Supercond Sci Technol* 2020;33:074005. DOI
  74. Soler L, Jareño J, Banchewski J, et al. Ultrafast transient liquid assisted growth of high current density superconducting films. *Nat Commun* 2020;11:344. DOI PubMed PMC
  75. Obradors X, Puig T. Coated conductors for power applications: materials challenges. *Supercond Sci Technol* 2014;27:044003. DOI
  76. Zeng L, Lu YM, Liu ZY, Chen CZ, Gao B, Cai CB. Surface texture and interior residual stress variation induced by thickness of YBa<sub>2</sub>Cu<sub>3</sub>O<sub>7-δ</sub> thin films. *J Appl Phys* 2012;112:053903. DOI
  77. Jia QX, Foltyn SR, Arendt PN, Smith JF. High-temperature superconducting thick films with enhanced supercurrent carrying capability. *Appl Phys Lett* 2002;80:1601-3. DOI
  78. Sun MJ, Yang WT, Liu ZY, et al. Ag doping effects on Y<sub>0.5</sub>Gd<sub>0.5</sub>Ba<sub>2</sub>Cu<sub>3</sub>O<sub>7-δ</sub> multilayers derived by low-fluorine metalorganic solution deposition. *Mater Res Express* 2015;2:096001. DOI
  79. Lin J, Yang W, Gu Z, et al. Improved epitaxial texture of thick YBa<sub>2</sub>Cu<sub>3</sub>O<sub>7-δ</sub>/GdBa<sub>2</sub>Cu<sub>3</sub>O<sub>7-δ</sub> films with periodic stress releasing. *Supercond Sci Technol* 2015;28:045001. DOI
  80. Lin J, Liu X, Cui C, et al. A review of thickness-induced evolutions of microstructure and superconducting performance of REBa<sub>2</sub>Cu<sub>3</sub>O<sub>7-δ</sub> coated conductor. *Adv Manuf* 2017;5:165-76. DOI
  81. Xu A, Delgado L, Heydari Gharahcheshmeh M, Khatri N, Liu Y, Selvamanickam V. Strong correlation between J<sub>c</sub> (T, H||c) and J<sub>c</sub> (77 K, 3T||c) in Zr-added (Gd, Y)BaCuO coated conductors at temperatures from 77 down to 20 K and fields up to 9 T. *Supercond Sci Technol* 2015;28:082001. DOI
  82. Selvamanickam V, Gharahcheshmeh MH, Xu A, Zhang Y, Galstyan E. Critical current density above 15 MA cm<sup>-2</sup> at 30 K, 3 T in 2.2 μm thick heavily-doped (Gd,Y)Ba<sub>2</sub>Cu<sub>3</sub>O<sub>x</sub> superconductor tapes. *Supercond Sci Technol* 2015;28:072002. DOI
  83. Malozemoff AP. Progress in American superconductor's HTS wire and optimization for fault current limiting systems. *Phys C Supercond Appl* 2016;530:65-7. DOI
  84. Majkic G, Pratap R, Paidpilli M, et al. In-field critical current performance of 4.0 μm thick film REBCO conductor with Hf addition at 4.2 K and fields up to 31.2 T. *Supercond Sci Technol* 2020;33:07LT03. DOI
  85. Dürrschnabel M, Aabdin Z, Bauer M, Semerad R, Prusseit W, Eibl O. DyBa<sub>2</sub>Cu<sub>3</sub>O<sub>7-x</sub> superconducting coated conductors with critical currents exceeding 1000 A cm<sup>-1</sup>. *Supercond Sci Technol* 2012;25:105007. DOI
  86. Campbell A, Everts J. Flux vortices and transport currents in type II superconductors. *Adv Phys* 1972;21:199-428. DOI
  87. Blatter G, Feigel'man MV, Geshkenbein VB, Larkin AI, Vinokur VM. Vortices in high-temperature superconductors. *Rev Mod Phys* 1994;66:1125-388. DOI
  88. Tachiki M, Takahashi S. Anisotropy of critical current in layered oxide superconductors. *Solid State Commun* 1989;72:1083-6. DOI
  89. Kwok WK, Welp U, Glatz A, Koshelev AE, Kihlstrom KJ, Crabtree GW. Vortices in high-performance high-temperature superconductors. *Rep Prog Phys* 2016;79:116501. DOI PubMed
  90. Karapetrov G, Belkin A, Novosad V, Iavarone M, Pearson JE, Kwok WK. Adjustable superconducting anisotropy in MoGe-Permalloy hybrids. *J Phys Conf Ser* 2009;150:052095. DOI
  91. Tang X, Zhao Y, Wu W, Grivel J. Effect of BaZrO<sub>3</sub>/Ag hybrid doping to the microstructure and performance of fluorine-free MOD method derived YBa<sub>2</sub>Cu<sub>3</sub>O<sub>7-x</sub> superconducting thin films. *J Mater Sci: Mater Electron* 2015;26:1806-11. DOI

92. Wang H, Ding F, Gu H, Zhang H, Dong Z. Microstructure and superconducting properties of (BaTiO<sub>3</sub>, Y<sub>2</sub>O<sub>3</sub>)-doped YBCO films under different firing temperatures. *Rare Met* 2017;36:37-41. DOI
93. Wang H, Ding F, Gu H, Zhang T. Strongly enhanced flux pinning in the YBa<sub>2</sub>Cu<sub>3</sub>O<sub>7-x</sub> films with the co-doping of BaTiO<sub>3</sub> nanorod and Y<sub>2</sub>O<sub>3</sub> nanoparticles at 65 K. *Chinese Phys B* 2015;24:097401. DOI
94. Jin S, Tiefel T, Kammlott G, Fastnacht R, Graebner J. Superconducting properties of YBa<sub>2</sub>Cu<sub>3</sub>O<sub>7-δ</sub> with partial rare earth substitution. *Physica C Supercond* 1991;173:75-9. DOI
95. Devi AR, Bai VS, Patanjali PV, Pinto R, Kumar NH, Malik SK. Enhanced critical current density due to flux pinning from lattice defects in pulsed laser ablated Y<sub>1-x</sub>Dy<sub>x</sub>Ba<sub>2</sub>Cu<sub>3</sub>O<sub>7-δ</sub> thin films. *Supercond Sci Technol* 2000;13:935-9. DOI
96. Jin L, Lu Y, Yan W, Yu Z, Wang Y, Li C. Fabrication of GdBa<sub>2</sub>Cu<sub>3</sub>O<sub>7-x</sub> films by TFA-MOD process. *J Alloys Compound* 2011;509:3353-6. DOI
97. Zhou H, Maiorov B, Wang H, et al. Improved microstructure and enhanced low-field J<sub>c</sub> in (Y<sub>0.67</sub>Eu<sub>0.33</sub>)Ba<sub>2</sub>Cu<sub>3</sub>O<sub>7-δ</sub> films. *Supercond Sci Technol* 2008;21:025001. DOI
98. Li M, Fang Q, Hu X, et al. Microstructures property and improved J<sub>c</sub> of Eu-doped YBa<sub>2</sub>Cu<sub>3</sub>O<sub>7-δ</sub> thin films by trifluoroacetate metal organic deposition process. *J Supercond Nov Magn* 2017;30:1137-43. DOI
99. Nie JC, Yamasaki H, Yamada H, Nakagawa Y, Develos-bagarinao K, Mawatari Y. Evidence for c-axis correlated vortex pinning in YBa<sub>2</sub>Cu<sub>3</sub>O<sub>7</sub> films on sapphire buffered with an atomically flat CeO<sub>2</sub> layer having a high density of nanodots. *Supercond Sci Technol* 2004;17:845-52. DOI
100. Aytug T, Paranthaman M, Gapud AA, et al. Enhancement of flux pinning and critical currents in YBa<sub>2</sub>Cu<sub>3</sub>O<sub>7-δ</sub> films by nanoscale iridium pretreatment of substrate surfaces. *J Appl Phys* 2005;98:114309. DOI
101. Baca FJ, Fisher D, Emergo RLS, Wu JZ. Pore formation and increased critical current density in YBa<sub>2</sub>Cu<sub>3</sub>O<sub>x</sub> films deposited on a substrate surface modulated by Y<sub>2</sub>O<sub>3</sub> nanoparticles. *Supercond Sci Technol* 2007;20:554-8. DOI
102. Mikheenko P, Sarkar A, Dang V, Tanner J, Abell J, Crisan A. c-Axis correlated extended defects and critical current in YBa<sub>2</sub>Cu<sub>3</sub>O films grown on Au and Ag-nano dot decorated substrates. *Physica C Supercond* 2009;469:798-804. DOI
103. Wang Y, Li Y, Liu L, Xu D. Improvement of flux pinning in GdBa<sub>2</sub>Cu<sub>3</sub>O<sub>7-δ</sub> thin film by nanoscale ferromagnetic La<sub>0.67</sub>Sr<sub>0.33</sub>MnO<sub>3</sub> pretreatment of substrate surface. *Ceram Int* 2018;44:225-30. DOI
104. Jha AK, Khare N, Pinto R. Influence of interfacial LSMO nanoparticles/layer on the vortex pinning properties of YBCO thin film. *J Supercond Nov Magn* 2014;27:1021-6. DOI
105. Matsui H, Ogiso H, Yamasaki H, et al. Enhancement of in-field critical current density by irradiation of MeV-energy ions in YBCO films prepared by fluorine-free metal-organic deposition. 24th International Symposium on Superconductivity (ISS). Tokyo, Japan: Elsevier Science; 2011. DOI
106. Matsui H, Ogiso H, Yamasaki H, et al. 4-fold enhancement in the critical current density of YBa<sub>2</sub>Cu<sub>3</sub>O<sub>7</sub> films by practical ion irradiation. *Appl Phys Lett* 2012;101:232601. DOI
107. Matsui H, Ootsuka T, Ogiso H, et al. Enhancement of critical current density in YBa<sub>2</sub>Cu<sub>3</sub>O<sub>7</sub> films using a semiconductor ion implanter. *J Appl Phys* 2015;117:043911. DOI
108. Huang D, Gu H, Shang H, et al. Enhancement in the critical current density of BaTiO<sub>3</sub>-doped YBCO films by low-energy (60 keV) proton irradiation. *Supercond Sci Technol* 2021;34:045001. DOI
109. Eley S, Leroux M, Rupich MW, et al. Decoupling and tuning competing effects of different types of defects on flux creep in irradiated YBa<sub>2</sub>Cu<sub>3</sub>O<sub>7-δ</sub> coated conductors. *Supercond Sci Technol* 2017;30:015010. DOI
110. Rupich MW, Sathyamurthy S, Fleshler S, et al. Engineered pinning landscapes for enhanced 2G coil wire. *IEEE Trans Appl Supercond* 2016;26:1-4. DOI
111. MacManus-Driscoll JL, Foltyn SR, Jia QX, et al. Strongly enhanced current densities in superconducting coated conductors of YBa<sub>2</sub>Cu<sub>3</sub>O<sub>7-x</sub> + BaZrO<sub>3</sub>. *Nat Mater* 2004;3:439-43. DOI PubMed
112. Gutiérrez J, Llordés A, Gázquez J, et al. Strong isotropic flux pinning in solution-derived YBa<sub>2</sub>Cu<sub>3</sub>O<sub>7-x</sub> nanocomposite superconductor films. *Nat Mater* 2007;6:367-73. DOI PubMed
113. Wang F, Tian H. BaZrO<sub>3</sub> (BZO) nanoparticles as effective pinning centers for YBa<sub>2</sub>Cu<sub>3</sub>O<sub>7-δ</sub> (YBCO) superconducting thin films. *J Mater Sci Mater Electron* 2019;30:4137-43. DOI
114. Selvamanickam V, Gharahcheshmeh MH, Xu A, Galstyan E, Delgado L, Cantoni C. High critical currents in heavily doped (Gd,Y)Ba<sub>2</sub>Cu<sub>3</sub>O<sub>x</sub> superconductor tapes. *Appl Phys Lett* 2015;106:032601. DOI
115. Xu A, Khatri N, Liu Y, et al. Broad temperature pinning study of 15 mol.% Zr-Added (Gd, Y)-Ba-Cu-O MOCVD coated conductors. *IEEE Trans Appl Supercond* 2015;25:1-5. DOI
116. Teranishi R, Otaguro K, Horita H, et al. Minimization of BaHfO<sub>3</sub> flux pinning centers in YBa<sub>2</sub>Cu<sub>3</sub>O<sub>y</sub> films by metal organic deposition process. *IEEE Trans Appl Supercond* 2016;26:1-3. DOI
117. Liu L, Wang W, Yao Y, Wu X, Lu S, Li Y. Formation of qualified BaHfO<sub>3</sub> doped Y<sub>0.5</sub>Gd<sub>0.5</sub>Ba<sub>2</sub>Cu<sub>3</sub>O<sub>7-δ</sub> film on CeO<sub>2</sub> buffered IBAD-MgO tape by self-seeding pulsed laser deposition. *Appl Surf Sci* 2018;439:1034-9. DOI
118. Dong Z, Ding F, Zhang J, et al. Enhanced flux pinning of solution-derived YBa<sub>2</sub>Cu<sub>3</sub>O<sub>7-x</sub> nanocomposite films with novel ultra-small BaMnO<sub>3</sub> nanocrystals. *Supercond Sci Technol* 2019;32:025004. DOI
119. Celentano G, Rizzo F, Augieri A, et al. YBa<sub>2</sub>Cu<sub>3</sub>O<sub>7-x</sub> films with Ba<sub>2</sub>Y(Nb,Ta)O<sub>6</sub> nano-inclusions for high-field applications. *Supercond Sci Technol* 2020;33:044010. DOI
120. Gondo M, Yoshida M, Yoshida Y, et al. Nanostructures and flux pinning properties in YBa<sub>2</sub>Cu<sub>3</sub>O<sub>7-y</sub> thin films with double perovskite

- Ba<sub>2</sub>LuNbO<sub>6</sub> nanorods. *J Appl Phys* 2021;129:195301. DOI
121. Hazelton DW, Selvamanickam V. SuperPower's YBCO coated high-temperature superconducting (HTS) wire and magnet applications. *Proc IEEE* 2009;97:1831-6. DOI
  122. Chen Y, Hazelton DW, Venkat S. High field magnet made of second generation high temperature superconducting wire. In 11th international conference on electrical machines and systems. Wuhan: Huazhong University of Science and Technology; 2008. DOI
  123. Yoon S, Cheon K, Lee H, et al. The performance of the conduction cooled 2G HTS magnet wound without turn to turn insulation generating 4.1T in 102mm bore. *Physica C Supercond* 2013;494:242-5. DOI
  124. Yoon S, Kim J, Cheon K, Lee H, Hahn S, Moon S. 26 T 35 mm all-GdBa<sub>2</sub>Cu<sub>3</sub>O<sub>7-x</sub> multi-width no-insulation superconducting magnet. *Supercond Sci Technol* 2016;29:04LT04. DOI
  125. Kim K, Bhattarai KR, Jang JY, et al. Design and performance estimation of a 35 T 40 mm no-insulation all-REBCO user magnet. *Supercond Sci Technol* 2017;30:065008. DOI
  126. Ding FZ, Zhang JY, Tan YF, et al. Development of a 4 T (46 K) 100 mm high-temperature superconducting coil made of homemade MOCVD-YBCO coated conductors. *Acta Phys Sin* 2018;67:20171491. DOI
  127. Kajita K, Iguchi S, Xu Y, et al. Degradation of a REBCO coil due to cleavage and peeling originating from an electromagnetic force. *IEEE Trans Appl Supercond* 2016;26:1-6. DOI
  128. Yanagisawa Y, Kajita K, Iguchi S, et al. 27.6 T generation using Bi-2223/REBCO superconducting coils. IEEE/CSC, 2016. Available from: [https://snf.ieeeesc.org/sites/ieeeesc.org/files/documents/snf/abstracts/edSTH42-HP112\\_Yanagisawa%2CY\\_27.6%20T\\_ed%20generation-final\\_071816.pdf](https://snf.ieeeesc.org/sites/ieeeesc.org/files/documents/snf/abstracts/edSTH42-HP112_Yanagisawa%2CY_27.6%20T_ed%20generation-final_071816.pdf) [Last accessed on 25 July 2022].
  129. Markiewicz WD, Larbalestier DC, Weijers HW, et al. Design of a superconducting 32 T magnet with REBCO high field coils. *IEEE Trans Appl Supercond* 2012;22:4300704. DOI
  130. Liu J, Song S, Wang Q, Zhang Q. Critical current analysis of an YBCO insert for ultrahigh-field all-superconducting magnet. *IEEE Trans Appl Supercond* 2016;26:1-6. DOI
  131. Liu J, Li Y. High-field insert with Bi- and Y-based tapes for 25-T all-superconducting magnet. *IEEE Trans Appl Supercond* 2016;26:1-5. DOI
  132. Liu J, Wang L, Qin L, Wang Q, Dai Y. Design, Fabrication, and test of a 12 T REBCO insert for a 27 T all-superconducting magnet. *IEEE Trans Appl Supercond* 2020;30:1-7. DOI
  133. Liu J, Wang Q, Qin L, et al. World record 32.35 tesla direct-current magnetic field generated with an all-superconducting magnet. *Supercond Sci Technol* 2020;33:03LT01. DOI
  134. Suetomi Y, Yoshida T, Takahashi S, et al. Quench and self-protecting behaviour of an intra-layer no-insulation (LNI) REBCO coil at 31.4 T. *Supercond Sci Technol* 2021;34:064003. DOI
  135. Bird M, Bole S, Eyssa Y, Gao B, Schneider-muntau H. Test results and potential for upgrade of the 45 T hybrid insert. *IEEE Trans Appl Supercond* 2000;10:439-42. DOI
  136. Hahn S, Kim K, Kim K, et al. 45.5-tesla direct-current magnetic field generated with a high-temperature superconducting magnet. *Nature* 2019;570:496-9. DOI PubMed
  137. Senatore C, Alessandrini M, Lucarelli A, Tediosi R, Uglietti D, Iwasa Y. Progresses and challenges in the development of high-field solenoidal magnets based on RE123 coated conductors. *Supercond Sci Technol* 2014;27:103001. DOI PubMed PMC
  138. Lu W, Fang J, Li D, Wu C, Guo L. The experimental research and analysis on the quench propagation of YBCO coated conductor and coil. *Physica C Supercond* 2013;484:153-8. DOI
  139. Angrisani Armenio A, Augieri A, Celentano G, et al. Stability measurements on YBCO coated conductors. *IEEE Trans Appl Supercond* 2008;18:1293-6. DOI
  140. Paidpilli M, Selvamanickam V. Development of RE-Ba-Cu-O superconductors in the US for ultra-high field magnets. *Supercond Sci Technol* 2022;35:043001. DOI
  141. Wang X, Caspi S, Dieterich DR, et al. A viable dipole magnet concept with REBCO CORC<sup>®</sup> wires and further development needs for high-field magnet applications. *Supercond Sci Technol* 2018;31:045007. DOI
  142. Macmanus-driscoll JL, Wimbush SC. Processing and application of high-temperature superconducting coated conductors. *Nat Rev Mater* 2021;6:587-604. DOI
  143. Sung H, Park M, Go B, Yu I. A study on the required performance of a 2G HTS wire for HTS wind power generators. *Supercond Sci Technol* 2016;29:054001. DOI
  144. Zhang, Lehner TF, Fukushima T, Sakamoto H, Hazelton DW. Progress in Production and performance of second generation (2G) HTS wire for practical applications. *IEEE Trans Appl Supercond* 2014;24:1-5. DOI
  145. Cai C, Chi C, Li M, et al. Advance and challenge of secondary-generation high-temperature superconducting tapes for high field applications. *Chin Sci Bull* 2019;64:827-41. DOI
  146. Ainslie M D, George A, Shaw R, et al. Design and market considerations for axial flux superconducting electric machine design. 11th European Conference on Applied Superconductivity (EUCAS). Genoa, Italy: IOP Publishing Ltd; 2013. DOI
  147. Molodyk A, Samoilnikov S, Markelov A, et al. Development and large volume production of extremely high current density YBa<sub>2</sub>Cu<sub>3</sub>O<sub>7</sub> superconducting wires for fusion. *Sci Rep* 2021;11:2084. DOI PubMed PMC
  148. Uglietti D. A review of commercial high temperature superconducting materials for large magnets: from wires and tapes to cables and conductors. *Supercond Sci Technol* 2019;32:053001. DOI